

1 Geology of the 'Sénia stone' from Ulldecona, Catalonia (Aptian,  
2 Maestrat Basin, Iberian Chain) and its implications for regional  
3 stratigraphy  
4

5 Telm Bover-Arnal\*, Ramon Salas

6 Departament de Mineralogia, Petrologia i Geologia Aplicada, Facultat de  
7 Ciències de la Terra, Universitat de Barcelona, Barcelona, Spain

8  
9 \* Corresponding author.

10 *E-mail address:* [telm.boverarnal@ub.edu](mailto:telm.boverarnal@ub.edu) (T. Bover-Arnal)

11  
12 **ABSTRACT**

13  
14 The municipality of the town of Ulldecona (Catalonia) is notable for extensive  
15 quarrying activities, which exploit limestone, popularly named Stone from  
16 Ulldecona, for ornamental and building purposes. The Stone from Ulldecona,  
17 commercially known as Sénia stone, is one of the most important ornamental  
18 and building stones quarried in Catalonia, and is used worldwide in all kinds of  
19 public and private buildings. Little is known about the geological nature of this  
20 stratigraphic interval of commercial value. Therefore, this study explores the  
21 geology of the Stone from Ulldecona in open pit quarries and natural outcrops.  
22 The Stone from Ulldecona consists of limestones of upper lower Aptian age,  
23 including wackestone, packstone and grainstone textures containing peloids,  
24 miliolids, *Palorbitolina lenticularis*, *Orbitolinopsis simplex*, *Paracoskinolina*  
25 *maynci*, *Lithocodium aggregatum*, *Choffatella decipiens*, *Salpingoporella*  
26 *muehlbergi*, *Chondrodonta*, *Toucasia carinata*, *Polyconites* sp. and *Mathesia*  
27 *darderi*. These platform carbonates rich in orbitolinids and rudists belong to the  
28 Villarroya de los Pinares Formation of the Maestrat Basin. Locally, the  
29 limestones are highly bioturbated and/or dolomitized. Dolomitic limestones,  
30 calcitic dolostones and dolostones are stratabound tabular geobodies with  
31 thicknesses of up to 60 metres. Dolomitic limestones and calcitic dolostones  
32 corresponding to initial and intermediate stages of dolomitization mainly exhibit  
33 isolated euhedral dolomite crystals or idiotopic mosaics. Dolostones (advanced  
34 dolomitization stages) are sucrose, exhibit vacuolar and cave porosities, and  
35 are characterized by idiotopic and hypidiotopic mosaics, which indicate  
36 temperatures lower than 50-60°C during dolomitization. Dolomite textures are  
37 mainly fabric-destructive and pervasive, but locally retentive and/or selective  
38 fabrics also occur. The limestones of the Villarroya de los Pinares Formation,  
39 the underlying marls of the Forcall Formation and the overlying marls and  
40 platform carbonates of the Benassal Formation examined can be arranged into  
41 two high-rank, low-frequency transgressive-regressive sequences. Similar  
42 coeval long-term transgressive-regressive trends have been reported from other

43 basins, indicating that eustatism largely controlled accommodation of the Aptian  
44 succession studied in Ulldecona.

45

#### 46 **Keywords**

47 carbonate platform, sequence stratigraphy, dolomitization, quarrying, Maestrat  
48 Basin, Aptian

49

#### 50 **1. Introduction**

51

52 The Stone from Ulldecona, commercialized as 'Sénia stone', is a  
53 limestone rock extracted from the Godall Range (Fig. 1), in the environs of the  
54 town of Ulldecona in southern Catalonia (NE Spain). In the area, the Stone from  
55 Ulldecona is cut in seven quarries by five different companies. Four local  
56 factories manufacture different products from it (Ajuntament d'Ulldecona, 2005).  
57 The Stone from Ulldecona is used as building/ornamental stone for both inner  
58 and outer parts in public and private construction, as well as for sculpture.  
59 Different commercial varieties exist based on the distinct colours and textures  
60 exhibited by this stone: Ulldecona, Ulldecona Cream, Sénia Jalo, Sénia Cream  
61 and Imperial (Martín et al., 2001; Navarro Torta, 2006). The hardness and  
62 versatility of the Stone from Ulldecona are of great value to engineers and  
63 architects, and it is produced and manufactured in different finishes such as cut,  
64 polished, flamed, ancient, sandy, bush hammered and honed (Ajuntament  
65 d'Ulldecona, 2005). It is probably the most important building and ornamental  
66 stone extracted in Catalonia.

67 Remarkable constructions in Barcelona where the Stone from Ulldecona  
68 was used include Casa Milà, also known as "La Pedrera" (Figs. 2A-B), and the  
69 Sagrada Família Temple (Figs. 2C-D), both edifices designed by the architect  
70 Antoni Gaudí, and World Heritage Sites designated by the United Nations  
71 Educational, Scientific and Cultural Organisation (UNESCO). Also in Barcelona,  
72 the shopping and entertainment centres Illa Diagonal (Fig. 2E) and Diagonal  
73 Mar are paved (Fig. 2F) and exterior wall cladded, respectively, with stone from  
74 Ulldecona (Ajuntament d'Ulldecona, 2005).

75 In Madrid, the Stone from Ulldecona was utilized for example in the  
76 Prado Museum to renew the floors of several rooms, as well as for interior and  
77 exterior wall cladding in the building of the Spanish Olympic Committee (Figs.  
78 3A-B). In the nearby city of Alcalá de Henares, designated as Human Heritage  
79 by UNESCO, the Stone from Ulldecona paves the renewed floors of the  
80 Magisterial Cathedral (Figs. 3C-D).

81 Furthermore, the Stone from Ulldecona was employed as wall cladding  
82 and/or pavement in notable constructions around the world such as the Olympic  
83 Stadium of Sevilla (Spain), the Northern Beach Promenade of Peníscola  
84 (Spain), the Ca Na Xica Hotel in Eivissa (Spain), the Puerta de Toledo in  
85 Ciudad Real (Spain), the Midsummer Place Shopping Centre in Central Milton  
86 Keynes (United Kingdom), the Tramway of Montpellier (France), the Swiss

87 Bank Corporation in Basel and the Nestlé Headquarters in Vevey (Switzerland),  
88 the Mondrian building and Les Jardins de la Couronne in Brussels (Belgium),  
89 the Amsterdam Arena Stadium (The Netherlands), the Rivierenstede building in  
90 Groningen (The Netherlands), the Supreme Education Council Headquarters in  
91 Doha (Qatar) and the Al Ain University of Science and Technology in Abu Dhabi  
92 (United Arab Emirates). In the United States of America, the Stone from  
93 Ulldecona paves floors and/or clads walls of the Helen and Martin Kimmel  
94 Center for University Life in Manhattan-New York, the Ritz Hotel in Aspen, the  
95 Park Regency in Atlanta, the Hilton Hotel and the cathedral of Los Angeles and  
96 the Miami Tower and the Four Seasons Hotel in Miami (Ajuntament  
97 d'Ulldecona, 2005).

98 Published studies of the Stone from Ulldecona are scarce and mainly  
99 restricted to the examination of the physical and mechanical properties of the  
100 rock and its pathologies (Torta Navarro, 2002, 2006; Fernández Burriel, 2009;  
101 Fernández et al., 2009). Only the explanatory notes of the Geological Map  
102 1:50.000 of Spain by Leyva et al. (1972) and the works by Fernández Burriel  
103 (2009) and Fernández et al. (2009) provide brief remarks on the geology and  
104 age of the Stone from Ulldecona. Leyva et al. (1972) give an Aptian (Lower  
105 Cretaceous) age to the marine limestone rocks quarried in the municipality of  
106 Ulldecona (*Comarca* of El Montsià). However, the analysis of the Aptian  
107 sedimentary record by these authors was not carried out in the area of  
108 Ulldecona but around 25 km to the W-SW, in the surroundings of the town of  
109 Xert (*Comarca* of El Baix Maestrat; Fig. 1B). Fernández Burriel (2009) and  
110 Fernández et al. (2009) characterize the Stone from Ulldecona as a limestone  
111 rock of Cretaceous age exhibiting wackestone, packstone, grainstone and  
112 dolosparite textures and containing skeletal components such as orbitolinids,  
113 miliolids and rudists.

114 The present work characterizes the petrology, sedimentology,  
115 diagenesis, stratigraphy and palaeontology of the Aptian platform carbonates  
116 extracted as Stone from Ulldecona, and investigates their exact age and  
117 distribution in the southern part of the Godall Range, also known as the Grossa  
118 Range. Moreover, the studied carbonate platform, which paves floors and clads  
119 walls around the world, is placed in regional and global contexts, and compared  
120 to coeval carbonate systems of the Tethys. The paper may be of relevance to  
121 those studying Cretaceous carbonate depositional systems, but also to those  
122 engaged in geological heritage, quarrying and construction activities.

123

124 ----- Figure 1 (width of page) near here -----

125 ----- Figure 2 (width of page) near here -----

126

127 **2. Geological setting**

129 The carbonate sedimentary succession studied gives rise to the Godall  
130 Range, which is located in the north-eastern part of the Maestrat Basin, in the  
131 eastern Iberian Chain (Fig. 1A). The Iberian Chain was formed by the Late  
132 Eocene-Early Miocene inversion of a rift system affecting the eastern Iberian  
133 Plate that resulted from two rifting cycles of Late Jurassic and Early Cretaceous  
134 ages (Nebot and Guimerà, 2018). The Late Jurassic rifting cycle was related to  
135 the opening of the North Atlantic, whereas the Early Cretaceous cycle  
136 corresponded to extensive intraplate deformation linked to the opening of the  
137 Bay of Biscay (Salas and Casas, 1993). These two rifting stages controlled the  
138 development of six major areas of preferential sedimentation or sedimentary  
139 basins in the north-eastern Iberia: i) Cantabrian, ii) Cameros, iii) Maestrat, iv)  
140 South-Iberian, v) Garraf, and vi) Columbrets (offshore) (Fig. 1A; Salas et al.,  
141 2001).

142 The syn-rift structure of the Maestrat Basin was formed by two systems  
143 of extensional listric faults generating a double roll-over geometry (Salas et al.,  
144 1995; Nebot and Guimerà, 2016). A northern system was formed by WNW-  
145 oriented normal listric faults dipping southwards (i.e., Herbers and Turmell  
146 faults; Fig. 1B), whereas a south-western system was oriented NW-SE and  
147 dipped towards the NE. This structure compartmentalised the Maestrat Basin  
148 into seven sub-basins: Aliaga, Galve, Oliete, Penyagolosa, Salzadella, El  
149 Perelló and Morella (Salas and Guimerà, 1996) (Fig. 1B). The Godall Range is  
150 located in the eastern sector of the Morella Sub-basin, which was the half-  
151 graben corresponding to the northern part of the Maestrat Basin (Fig. 1B).

152 In the Maestrat Basin, during the Late Jurassic-Early Cretaceous time  
153 period, sedimentation occurred in shallow-marine carbonate settings, which was  
154 interrupted by inputs of coastal siliciclastics and continental sedimentation  
155 during the latest Jurassic (Purbeck Facies), the Barremian (Weald Facies and  
156 freshwater carbonates) and the Albian (Utrillas Facies). The thickness of the  
157 Upper Jurassic-Lower Cretaceous syn-rift succession is superior to 4 km in  
158 depocentral areas.

159 In the Morella Sub-basin, the Aptian lithostratigraphic units overlie the  
160 upper Barremian succession, which includes the shallow-marine carbonates  
161 and marls rich in oysters of the Artoles Formation, the continental red clays and  
162 sandstones containing dinosaur remains of the Morella Formation, the coastal  
163 mixed carbonate-siliciclastic deposits of the Cervera del Maestrat Formation,  
164 and the marine sandstones, sandy limestones, marls and limestones rich in  
165 *Palorbitolina lenticularis* of the Xert Formation (Fig. 4) (Bover-Arnal et al., 2016).  
166 From older to younger, the Aptian units correspond to the basinal marls, marly-  
167 limestones and limestones with *Palorbitolina lenticularis* and ammonoids of the  
168 Forcall Formation, the platform carbonates with rudists and corals of the

169 Villarroya de los Pinares Formation, and the marls and limestones with rudists,  
170 corals and *Mesorbitolina texana* of the Benassal Formation (Fig. 4) (Canérot et  
171 al., 1982; Salas, 1987; Salas et al., 1995; Bover-Arnal et al., 2014, 2016). The  
172 Aptian succession is overlain by the sandstones and clays of the Utrillas Facies  
173 (Fig. 4) (Canérot et al., 1982), which are Albian in age (Garcia et al., 2014;  
174 Bover-Arnal et al., 2016) and include the Escucha and Utrillas formations. In the  
175 Godall Range, the Utrillas Facies is locally capped by the Cenomanian marine  
176 limestones and dolostones of the Mosqueruela Formation (Figs. 5-6) (Canérot  
177 et al., 1982).

178 ----- Figure 3 (width of page) near here -----

179 ----- Figure 4 (width of page) near here -----

### 180 **3. Materials and methods**

181

182 The Early Cretaceous carbonate sedimentary succession of the southern  
183 part of the Godall Range (Grossa Range) was investigated by means of field  
184 and laboratory work. Fieldwork involved the generation of an original 1:25,000  
185 scale geological map of the area (Fig. 5), the logging and sampling of a  
186 representative stratigraphic section (Figs. 7-8), lithofacies description,  
187 macrofossil identification and taxonomic determinations of rudist bivalves,  
188 mapping of lithofacies architecture on panoramic photomosaics of the quarries,  
189 and random sampling within the quarries. The geological scheme was created  
190 over a 1:25,000 scale topographic base of Catalonia by the Institut Cartogràfic i  
191 Geològic de Catalunya (sheet 62-41; available at <http://www.icgc.cat>).

192 The laboratory work included the production of three geological cross-  
193 sections (Fig. 6) to recognize the general structural framework and stratigraphic  
194 relationships of the study area, as well as the analysis of microfacies and  
195 determination of microfossils on 64 thin sections produced from the samples  
196 collected in the field. The carbonate rocks examined were classified following  
197 Dunham (1962) and Embry and Klovan (1971). The taxonomic determinations  
198 of rudists, orbitolinids and of other benthic foraminifera, which were used to  
199 determine the age of the rocks investigated, follow the biostratigraphic analyses  
200 by Masse (2003), Skelton (2003), Bover-Arnal et al. (2010, 2016), Skelton et al.  
201 (2010), Schroeder et al. (2010), Cherchi and Schroeder (2013), Skelton and Gili  
202 (2012) and Steuber et al. (2016). The transgressive-regressive sequence-  
203 stratigraphic arrangement of the sedimentary record studied follows the  
204 nomenclature proposed by Catuneanu et al. (2011).

205

### 206 **4. Geological scheme and cross-sections**

207

208           In this chapter, a geological scheme of the southern part of the Godall  
209 Range is presented (Fig. 5). Due to a requisition by a funding agency of this  
210 study, the original geological scheme was simplified and only six cartographic  
211 units are characterized. From base (older) to top (younger), these stratigraphic  
212 units correspond to the Forcall Formation (lower Aptian), the Villarroya de los  
213 Pinares Formation (upper lower Aptian), the Benassal Formation (uppermost  
214 lower Aptian-upper Aptian), the Escucha Formation (Albian), the Mosqueruela  
215 Formation (Cenomanian) and undifferentiated Quaternary deposits.

216           Three representative schematic geological cross-sections of the Grossa  
217 Range (Fig. 6) were produced from the geological map. The location of the  
218 cross-sections can be seen in Figure 5. The A-A' cross-section is a SE-NW-  
219 oriented profile that displays the stratigraphic relationships between the Forcall,  
220 Villarroya de los Pinares and Benassal formations (Fig. 6). The B-B' cross-  
221 section is also oriented in a SE-NW direction and cuts the highest peak in the  
222 area, Lo Molló (Fig. 6). The C-C' cross-section follows a NE-SW direction and  
223 crosses the Grossa Range from the site of Mas del Dengo to Les Tosses (Fig.  
224 6).

225           An anticline and a syncline with SW-NE orientation characterize the  
226 structure of the area studied (Fig. 5). These regional folds exhibit the same SW-  
227 NE direction as the Godall Range (Fig. 5). With the exception of the strata close  
228 to the axial planes of the folds, the dips of the sedimentary record analysed are  
229 mainly gentle between 3 and 20 degrees, with a marked component to the NW  
230 (Figs. 5-6).

231           The Villarroya de los Pinares Formation is the main outcropping  
232 lithostratigraphic unit in the southern part of the Godall Range (Figs. 5-6). The  
233 building/ornamental stone industries, which quarry the lower part of the  
234 Villarroya de los Pinares Formation, are essentially located in the SE edge of  
235 the Godall Range, following the overall SW-NE structural trend (Fig. 5). The  
236 Forcall Formation, which stratigraphically underlies the Villarroya de los Pinares  
237 Formation (Fig. 4), crops out locally around the intersection between the axial  
238 plane of the anticline fold mapped and the road TV-3313, in the NE part of the  
239 study area. Strata belonging to the Benassal Formation, which stratigraphically  
240 overlies the Villarroya de los Pinares Formation (Fig. 4), is also locally  
241 preserved in the NE part of the Grossa Range, in the Mas del Dengo site (Figs.  
242 5-6). In addition, in the most western edge of the area investigated, in Les  
243 Tosses hillock, Albian and Cenomanian deposits, which respectively  
244 correspond to the Utrillas Facies and the Mosqueruela Formation,  
245 unconformably overlie the Aptian succession.

246 ----- Figure 5 VERTICAL (same size as Fig. 6) near here -----

247 ----- Figure 6 VERTICAL (same size as Fig. 5) near here -----

## 248 **5. Stratigraphic log**

249

250 The representative stratigraphic column of the Grossa Range (Figs. 7-8)  
251 was mainly measured along the TV-3313 road that goes from Uldecona to the  
252 town of Godall (Fig. 5). This road cuts the most complete section that has been  
253 recognized in the area, including the upper part of the Forcall Formation (25 m-  
254 thick), the whole of the Villarroya de los Pinares Formation (296 m-thick) and  
255 the basal part of the Benassal Formation (3 m-thick). These lithostratigraphic  
256 units correspond to the three marine formations of the Aptian of the Maestrat  
257 Basin (see Fig. 4 for the chronostratigraphy of the Early Cretaceous of the  
258 Maestrat Basin). The upper part of the Villarroya de los Pinares Formation, and  
259 the preserved deposits of the Benassal Formation have been measured on the  
260 hill of Mas del Dengo, adjacent to the TV-3313 road, as shown in Figure 5.

261

262 ----- Figure 7 (width of page) near here -----

263 ----- Figure 8 (width of page) near here -----

## 264 **6. Facies succession and fossil content**

265

266 The sedimentary succession examined begins with the marls of the  
267 Forcall Formation (Figs. 7, 9A). These marls crop out locally in the axial part of  
268 an antiform structure that crosses the area studied from the NE to the SW (see  
269 Fig. 5). Macrofossils were not found within the marls. At the upper part of the  
270 Forcall Formation, two limestone layers with wackestone and packstone  
271 textures contain miliolids, the bivalve *Chondrodonta* and other skeletal  
272 components (Fig. 7).

273 Above, the platform carbonates of the Villarroya de los Pinares  
274 Formation exhibit an initial section made up of marly-limestones and limestones  
275 rich in orbitolinids (between 25 and 38 m of the succession) (Figs. 7, 9B). Then,  
276 between 38 and 135 m, the succession consists basically of limestones with  
277 wackestone (Fig. 9C), packstone (Fig. 9D) and grainstone (Fig. 9E) textures  
278 rich in miliolids, orbitolinids, textularids, other benthic foraminifers,  
279 dasycladacean algae, oysters, nerineid gastropods, other gastropods,  
280 echinoderms and peloids. Packstone, floatstone and rudstone textures  
281 containing *Chondrodonta* and rudist bivalves in life position are locally present.  
282 Interbedded dolostones, calcitic dolostones, dolomitic limestones, as well as  
283 intensively bioturbated levels, also occur (Figs. 7, 9F). From 135 to 155 m, the  
284 succession is formed by packstone, grainstone and floatstone limestones

285 characterized by the presence of abundant rudists and *Chondrodonta* (Figs. 7,  
286 10A). Locally, colonies of scleractinian corals were recognized (Fig. 10B).

287 The stratigraphic interval quarried as an ornamental/building stone in the  
288 Grossa Range corresponds to the succession between 38 and 155 m (Figs. 7,  
289 10C). The wackestone (Fig. 9C), packstone (Fig. 9D) and grainstone (Fig. 9E)  
290 textures dominated by peloids, miliolids and dasycladaceans are the most  
291 prized microfacies as an ornamental and building rock in the quarries of the  
292 Grossa Range as they exhibit a gray or homogeneous cream tone without  
293 visible skeletal components. The bioturbated levels or beds including bivalves  
294 such as rudists and *Chondrodonta* are not as commercially attractive, but are  
295 marketed as well. When skeletal components are visible, the rock is considered  
296 unsightly. Bioturbated levels (Fig. 9F), apart from being considered unattractive,  
297 are less consistent, break more easily, and it is not possible to give a  
298 homogenous polish to the rock. A recent penetrative karst system (Fig. 10D)  
299 developed in the limestones of the lower part of the Villarroya de los Pinares  
300 Formation is also problematic for the quarrying industry of the area.

301 Above 155 m, the succession is intensively dolomitized until 215 m (Fig.  
302 7). From 215 to 322 m, the Villarroya de los Pinares Formation is made up of  
303 floatstone to rudstone limestones dominated by rudists (Figs. 7). Accordingly, in  
304 the Grossa Range, the Villarroya de los Pinares Formation can be subdivided  
305 into three units; a lower and an upper limestone-dominated units, which are  
306 separated by a middle dolostone interval (Fig. 7). The stratigraphic interval of  
307 mining interest from which the building and ornamental stone from Ulldecona is  
308 extracted corresponds to the limestones and dolomitic limestones of the lower  
309 part of the Villarroya de los Pinares Formation (Fig. 7).

310 The fossil content recognized within the Villarroya de los Pinares  
311 Formation, which gives rise to the Grossa Range, includes *Palorbitolina*  
312 *lenticularis* (Blumenbach) (Fig. 11A), *Orbitolinopsis simplex* (Henson) (Fig.  
313 11B), *Paracoskinolina maynci* (Chevalier) (Fig. 11C), *Choffatella decipiens*  
314 Schlumberger (Fig. 11D), *Lithocodium aggregatum* Elliott (Fig. 11E),  
315 *Salpingoporella muehlbergi* (Lorenz) (Fig. 11F), *Chondrodonta* Stanton (Fig.  
316 10A), *Toucasia carinata* (Matheron) (Fig. 12A), *Mathesia darderi* (Astre) (Fig.  
317 12B) and *Polyconites* sp. (Figs. 12C-D). The *Polyconites* sp. surveyed are  
318 characterized by exhibiting a modest size (between 2 and 4 cm in height), a  
319 relatively thick aragonite wall and a flattened left valve (Fig. 12D).

320 At 322 m, a 2 m-thick interval of basinal marls, which correspond to the  
321 base of the Benassal Formation (Fig. 13A), cover a hardground exhibiting  
322 borings of lithophagid bivalves and iron mineralizations (Figs. 13B-C). This  
323 hardground is located at the top of a rudist-bearing limestone bed belonging to  
324 the Villarroya de los Pinares Formation (Fig. 7). Above the marls, limestones  
325 with orbitolinids and bouquets of polyconitid rudists occur (Figs. 7, 13D).

326  
327

----- Figure 9 (width of page) near here -----

328 ----- Figure 10 (width of page) near here -----

329 ----- Figure 11 (width of page) near here -----

330 ----- Figure 12 (width of page) near here -----

331 ----- Figure 13 (width of page) near here -----

332

## 333 **7. Dolomites and dolomitization**

334

335 The Villarroya de los Pinares Formation in the Grossa Range consists of  
336 an alternation of marls, marly-limestones, limestones, dolomitic limestones,  
337 calcitic dolostones and dolostones. The stratigraphic interval with dolomites is  
338 mainly located in the middle part of the formation, between 155 and 216 m in  
339 the section measured on the TV-3313 road that goes from Ulldecona to Godall  
340 (Figs. 5, 7).

341 The dolomite levels are stratabound tabular geobodies, with thicknesses  
342 that vary from a few decimetres to tens of metres (up to 61 m in the type section  
343 displayed in Figure 7). This latter stratigraphic interval of between approximately  
344 40 and 60 meters (Fig. 14A) is a continuous level throughout the Grossa  
345 Range. The dolomite interval caps the stratigraphic succession extracted as an  
346 ornamental/building stone in active (e.g., Ebre, Sant Joan and Godall) and  
347 abandoned (e.g., El Xertolí) quarries in the municipality of Ulldecona (Fig. 14A),  
348 and is well exposed along the TV-3313 road that goes from Ulldecona to Godall  
349 (Figs. 5, 7).

350 The dolomite level of the middle part of the Villarroya de los Pinares  
351 Formation (Fig. 7) also presents the highest degree of dolomitization recognized  
352 within the Grossa Range. Dolostones are sucrose, beige, and exhibit vacuolar  
353 (Fig. 14B) and cave (Fig. 14C) porosities. At the base of this dolostone level,  
354 ghosts of skeletal components such as orbitolinids and rudists can be  
355 recognized. These dolostones are not extracted as ornamental/building rocks in  
356 the quarries of the area, but must be removed by the companies to reach the  
357 underlying limestone that is of economic interest (Fig. 14A).

358 Decimetric to metric stratabound tabular levels of dolomitic limestones  
359 and calcitic dolostones are recurrent within the Villarroya de los Pinares  
360 Formation (Fig. 14D) below the thick and widespread dolostone reference level  
361 (Figs. 7, 14A). These decimetric and metric dolomitic levels of the lower middle  
362 part of the Villarroya de los Pinares Formation are darker than the limestone  
363 with miliolids, peloids, rudists and *Chondrodonta* extracted as an  
364 ornamental/building rock, and are therefore easily recognizable inside the  
365 quarries of the area studied (Fig. 14D). When these stratabound decimetric to  
366 metric levels of dolomitic limestones and calcitic dolostones are cross-cut by

367 fractures, the circulation of calcite-rich meteoric waters calcitize the dolomitic  
368 hostrock, and the darker colour exhibited by the dolomitic limestones and  
369 calcitic dolostones diffuses around the fracture (Fig. 10D).

370 The dolomitic limestones, calcitic dolostones and dolostones found in the  
371 succession studied are of secondary origin, and formed by replacement during  
372 diagenesis (burial). The rocks investigated show different degrees of  
373 dolomitization; initial stages (Fig. 15A), intermediate stages (Fig. 15B) and  
374 advanced stages (Figs. 15C-D). Initial and intermediate stages of dolomitization  
375 mainly show idiotopic mosaics with euhedric crystals (rhomboids), and a  
376 destructive and pervasive fabric. Locally, retentive (i.e., ghosts and mouldic  
377 porosity of orbitolinids and rudists) and/or selective (mainly micritic matrix-  
378 selective dolomitization) fabrics have also been observed. Advanced  
379 dolomitization stages show a destructive and pervasive fabric with idiotopic (Fig.  
380 15C) and hypidiotopic (Fig. 15D) mosaics exhibiting euhedral and subhedral  
381 crystals.

382

383 ----- Figure 14 (width of page) near here -----

384 ----- Figure 15 (width of page) near here -----

385

386

## 387 **8. Discussion**

388

### 389 *8.1. Age of the succession*

390

391 In the Grossa Range, the Villarroya de los Pinares Formation, which  
392 includes the stratigraphic interval commercialized as an ornamental/building  
393 rock by the quarries located in the municipality of Ulldecona, contains  
394 *Palorbitolina lenticularis* (Figs. 9B, 11A) and *Orbitolinopsis simplex* (Figs. 9D,  
395 11B). *Palorbitolina lenticularis* has a stratigraphic distribution from the upper  
396 Barremian to the lower Aptian (Schroeder et al., 2010; Cherchi and Schroeder,  
397 2013), whereas *Orbitolinopsis simplex* ranges from the upper lower Aptian to  
398 the upper Aptian (Masse, 2003; Schlagintweit et al., 2016). Accordingly, the age  
399 of the Villarroya de los Pinares Formation is upper lower Aptian. In this regard,  
400 the occurrence of *Paracoskinolina maynci* (Fig. 11C), *Choffatella decipiens* (Fig.  
401 11D), *Lithocodium aggregatum* (Fig. 11E), *Salpingoporella muehlbergi* (Fig.  
402 11F), *Chondrodonta* (Fig. 10A), *Toucasia carinata* (Fig. 12A), *Polyconites* sp.  
403 (Fig. 12D) and *Mathesia darderi* (Fig. 12B) is also in accordance with an upper  
404 lower Aptian (Bedoulian) age (e.g., Arnaud et al., 1998; Bernaus et al., 2003;  
405 Skelton, 2003; Bover-Arnal et al., 2010, 2011, 2015, 2016; Skelton et al., 2010;  
406 Schlagintweit and Bover-Arnal, 2012; Skelton and Gili, 2012; Schlagintweit et  
407 al., 2010, 2013, 2016; Granier et al., 2013; Gili et al., 2016; Steuber et al., 2016;

408 Posenato et al., 2018). In addition, the observed *Polyconites* rudists exhibit a  
409 relatively thick aragonite wall (Fig. 12D), a flattened left valve, and a modest  
410 size, typical characteristics of specimens of late Early Aptian age (*Dufrenoyia*  
411 *furcata* ammonoid zone; see Fig. 4) (Skelton et al., 2010; Pascual-Cebrian,  
412 2014; Pascual-Cebrian et al., 2016) and hence, most likely to be *Polyconites*  
413 *hadriani* Skelton et al. (Skelton et al., 2010).

414 On the other hand, age-diagnostic fossils were not found within the  
415 Forcall Formation, which crops out locally in a TV-3313 road cut intersecting the  
416 axial part of a major antiform structure (see Figs. 5-7, 9A). In all the sub-basins  
417 of the Maestrat Basin, including the Morella Sub-basin where the area studied is  
418 found (Fig. 1B), the age of the Forcall Formation has been determined by  
419 means of ammonites as lower Aptian (Weisser, 1959; Canérot et al., 1982;  
420 Salas, 1987; Salas et al., 2001; Vennin and Aurell, 2001; Moreno-Bedmar et al.,  
421 2009, 2010, 2014; Bover-Arnal et al., 2010, 2015, 2016; Ossó et al., 2018).  
422 More precisely, the boundary between the Barremian and the Aptian is located  
423 within the lower, non-basal part of the Forcall Formation (Moreno-Bedmar and  
424 Garcia, 2011; Garcia et al., 2014; Bover-Arnal et al., 2016; see Fig. 4).  
425 Accordingly, a lower Aptian age for the Forcall Formation in the area of  
426 Uldecona is assumed.

427 The age of the Benassal Formation has not been possible to determine  
428 in the Grossa Range, either. The lower part of this formation is preserved at  
429 Mas del Dengo (Figs. 5-7). In the Maestrat Basin, the boundary between the  
430 early and the late Aptian is stratigraphically located in the lower, non-basal part  
431 of the first marl interval of the Benassal Formation (Bover-Arnal et al., 2014,  
432 2016; see Fig. 4). In the Morella and Galve sub-basins, the lower, non-basal  
433 part of this first marly horizon of the Benassal Formation contains ammonites of  
434 the *Dufrenoyia furcata* Zone (uppermost lower Aptian) (Moreno-Bedmar et al.,  
435 2012a; Bover-Arnal et al., 2014, 2016; Garcia et al., 2014). According to this  
436 chronostratigraphic framework (Fig. 4), the boundary between the early and late  
437 Aptian in the Grossa Range is also assigned to the lower, non-basal part of the  
438 first marl interval of the Benassal Formation (Figs. 7, 13A).

439 The Escucha and Mosqueruela formations mapped in Les Tosses area  
440 (Figs. 5-6), are ascribed respectively to the lower Albian according to Moreno-  
441 Bedmar et al. (2008), Garcia et al. (2014) and Bover-Arnal et al. (2016), and to  
442 the Cenomanian in accordance with Canérot et al. (1982).

443

## 444 8.2. Changes in accommodation and platform evolution

445

446 Stratal terminations or stacking patterns were not recognized along the  
447 succession studied and thus it was not possible to characterize systems tracts.  
448 Accordingly, the changes in accommodation that controlled sedimentation  
449 during the Aptian in this eastern part of the Maestrat Basin (Fig. 1B) are  
450 discussed herein by means of a transgressive-regressive analysis (*sensu*  
451 Johnson and Murphy, 1984). The transgressive-regressive sequence

452 stratigraphic approach is based on the identification of maximum-regressive and  
453 maximum-flooding surfaces, which mark large-scale changes of facies trends  
454 from shallowing- to deepening-upwards, and from deepening- to shallowing-  
455 upwards, respectively (e.g., Catuneanu et al., 2011).

456 The marls of the Forcall Formation have been mainly interpreted  
457 throughout the Maestrat Basin as transgressive deposits (Malchus et al., 1995;  
458 Vennin and Aurell, 2001; Bover-Arnal et al., 2009, 2010, 2014, 2015, 2016;  
459 Embry et al., 2010). In this respect, this marly unit contains relatively deep-  
460 water biota such as ammonoids and nautiloids (Weisser, 1959; Martínez and  
461 Grauges, 2006; Moreno-Bedmar et al., 2009, 2010; Grauges et al., 2010;  
462 Garcia et al., 2014; Lehmann et al., 2017), and is regionally overlain by  
463 shallower-water platform carbonates rich in rudists and corals (e.g., Malchus et  
464 al., 1995; Bover-Arnal et al., 2010, 2016) that belong to the Villarroya de los  
465 Pinares Formation (Salas, 1987; Canérot et al., 1982; Fig. 4).

466 In the area studied, the Villarroya de los Pinares Formation begins with  
467 an alternation of marls and limestones with wackestone, packstone and  
468 grainstone textures mainly containing peloids, orbitolinids, miliolids,  
469 *Chondrodonta* and oysters. Upwards in the succession, this lithostratigraphic  
470 unit progressively evolves into floatstones and rudstones dominated by rudists  
471 (Fig. 7). Aptian rudist-bearing limestones indicate platform-top environments  
472 (e.g., Skelton and Gili, 2012; Bover-Arnal et al., 2015; Gili et al., 2016).  
473 Therefore, the lithofacies evolution recorded by the Villarroya de los Pinares  
474 Formation in Ulldecona marks a long-term progressive shallowing-upwards  
475 trend from distal platform-slope to more proximal platform-top settings, which is  
476 in accordance with a regressive context (Fig. 7).

477 The maximum flooding surface bounding the transgressive marls of the  
478 Forcall Formation from the overlying regressive deposits is interpreted to  
479 correspond to the base of the first limestone level logged at metre 21, in the  
480 uppermost part of the Forcall Formation (Fig. 7). This limestone bed is made up  
481 of a packstone texture containing relatively shallow-water biota such as miliolids  
482 and *Chondrodonta*, and is interpreted to represent the first shedding arrival in  
483 the basin of platform top carbonate from a carbonate prograding system. In  
484 seismic sequence stratigraphy, the maximum flooding surface is placed at the  
485 first downlapping clinof orm recorded above transgressive deposits (e.g.,  
486 Catuneanu et al., 2011).

487 At 322 m (Fig. 7), at the top of a rudist-dominated limestone layer, a  
488 hardground exhibiting borings of lithophagous bivalves and iron mineralizations  
489 occurs (Figs. 13B-C). Physical signs of subaerial exposure such as karst  
490 features were not observed in this latter stratigraphic surface. The hardground  
491 is overlain by a 2 m-thick basinal marl interval, which belongs to the base of the  
492 Benassal Formation (Fig. 13A), and thus marks the drowning of the Villarroya  
493 de los Pinares Formation carbonate platform (Figs. 7, 13B-C). Accordingly, this  
494 hardground surface is interpreted as a maximum regressive surface which

495 bounds regressive platform carbonates of the Villarroya de los Pinares  
496 Formation from transgressive marls of the Benassal Formation (Fig. 7).

497 Above the marl interval, the presence of limestones with mesorbitolinids  
498 and *Polyconites* rudists in life position (Fig. 13D) indicates a renewed carbonate  
499 platform growth and thus, a marine regressive context (Fig. 7). These platform  
500 carbonates, which have been preserved locally from recent erosion (Figs. 5-6),  
501 still belong to the lower part of the Benassal Formation (Fig. 4; see Bover-Arnal  
502 et al., 2016). The maximum flooding surface between the transgressive marls  
503 and the regressive carbonates of the Benassal Formation was placed at the  
504 base of the first limestone layer above the marls (ca. 324 m; Fig. 7) following  
505 the same criterion explained above.

506 Accordingly, two low-frequency (high-rank; *sensu* Catuneanu et al.,  
507 2011) transgressive-regressive sequences were characterized along the Aptian  
508 succession of the Grossa Range. These sequences are of lower Aptian and  
509 uppermost lower-lower upper Aptian age, respectively. The transgressive units  
510 correspond to marls, whereas the regressive deposits are platform carbonates  
511 dominated by rudist bivalves.

512  
513

### 514 *8.3. Regional and global significance of interpretations*

515

516 The transgressive marls of the Forcall Formation identified in the Grossa  
517 Range (Figs. 5-7, 9A) can be regionally traced throughout the Maestrat Basin  
518 (Fig. 4; Canérot et al., 1982; Salas, 1987; Salas et al., 2001; Moreno-Bedmar et  
519 al., 2009, 2010; Garcia et al., 2014; Bover-Arnal et al., 2016). These marls,  
520 which frequently alternate with marly-limestones and limestones, have been  
521 interpreted as basinal deposits, and are commonly rich in *Palorbitolina*  
522 *lenticularis*, ammonoids, nautiloids and sponge spicules (e.g., Weisser, 1959;  
523 Canérot et al., 1982; Salas, 1987; Vennin and Aurell, 2001; Martínez and  
524 Grauges, 2006; Moreno-Bedmar et al., 2009, 2010; Grauges et al., 2010;  
525 Embry et al., 2010; Garcia et al., 2014; Bover-Arnal et al., 2016; Lehmann et al.,  
526 2017). Along the same lines, coeval relatively deep-water lithostratigraphic units  
527 are found in other basins of the Iberian Chain (Fig. 1A). For example, the  
528 Margues de Vallcarca Unit in the Garraf Basin (Fig. 1A; Moreno-Bedmar et al.,  
529 2016) or the lower and middle parts of the Malacara Member in the South  
530 Iberian Basin (Fig. 1A; Mas, 1981).

531 In the Maestrat Basin, the deposition of the marls of the Forcall  
532 Formation constitutes the acme of a large-scale transgression that commenced  
533 with the deposition of the marine sandstones, sandy-limestones and limestones  
534 with *Palorbitolina lenticularis* of the underlying Xert Formation during the Late  
535 Barremian (Fig. 4; Bover-Arnal et al., 2010, 2016). This high-rank transgressive  
536 trend led to the oceanic anoxic event 1a (OAE1a), which is recorded within the  
537 Forcall Formation (*Deshayesites forbesi* ammonoid zone) in the Maestrat Basin

538 (Moreno-Bedmar et al., 2009; Bover-Arnal et al., 2010, 2011, 2016; Embry et  
539 al., 2010; Cors et al., 2015).

540 High-rank transgressive trends of Early Aptian age characterized by the  
541 deposition of basin marls were also recorded in nearby basins such as the  
542 Organyà Basin in the southern Pyrenees (Bernaus et al., 2003; Sanchez-  
543 Hernandez et al., 2014), the Prebetic Domain in southeast Iberia (Vilas et al.,  
544 1995; Castro et al., 2008; Moreno-Bedmar et al. 2012b), the Basque-Cantabrian  
545 Basin in northern Iberia (García-Mondéjar et al., 2009; Schlagintweit et al.,  
546 2016; Fernández-Mendiola et al., 2017), and the Southeast France Basin  
547 (Masse and Fenerci-Masse, 2011; Pictet et al., 2015). Along the same lines,  
548 coeval large-scale transgressions have been reported from other parts of the  
549 Tethys (Föllmi et al., 1994; Sahagian et al., 1996; Hardenbol et al., 1998; Pittet  
550 et al., 2002; Wissler et al., 2003; Husinec and Jelaska 2006; Husinec et al.,  
551 2012; Hfaiedh et al., 2013; Suarez-Gonzalez et al., 2013; Wilmsen et al., 2015;  
552 Zorina et al., 2016), as well as from other basins worldwide (Cooper, 1977; Haq,  
553 2016).

554 The regressive platform carbonates of the Villarroya de los Pinares  
555 Formation studied are also widespread in the Maestrat Basin (Fig. 4; Canérot et  
556 al., 1982; Salas, 1987). Throughout the Maestrat Basin, besides rudists and  
557 *Chondrodonta*, this formation also includes abundant corals, orbitolinids and  
558 miliolids (Salas, 1987; Malchus et al., 1995; Vennin and Aurell, 2000; Bover-  
559 Arnal et al., 2010, 2012, 2014). The Villarroya de los Pinares Formation  
560 cropping out in the Grossa Range is coeval with the platform carbonates of the  
561 same formation that form the nearby hillock called La Mola de Xert (Fig. 1B;  
562 Salas, 1987; Malchus et al., 1995), which is located 25 km to the W-SW, in the  
563 environs of the town of Xert (*Comarca* of El Baix Maestrat). (The town of Xert  
564 and La Mola de Xert should not be confused with the Xert Formation of  
565 Barremian age (Fig. 4; see Bover-Arnal et al., 2016)). The two successions  
566 characterized by the presence of rudists and *Chondrodonta* were probably part  
567 of the same carbonate platform system. The limestones of the Villarroya de los  
568 Pinares Formation of La Mola de Xert have been also traditionally exploited as  
569 an ornamental stone, which is commercially known as Crema Jaspe. The  
570 succession exploited in La Mola de Xert is correlatable with the rudist-  
571 dominated upper part of the Villarroya de los Pinares Formation in Ulldecona  
572 (Fig. 7). On the other hand, the rock extracted in Ulldecona, which belongs to  
573 the lower part of the Villarroya de los Pinares Formation (Fig. 7), correlates with  
574 deeper-water micritic limestones containing sponge spicules, *Dufrenoyia furcata*  
575 and orbitolinids in La Mola de Xert (see Salas, 1987; Malchus et al., 1995).  
576 Accordingly, the Aptian succession of La Mola de Xert represents more distal  
577 depositional environments than the succession studied in the Grossa Range.  
578 Similar to the Grossa Range, the Villarroya de los Pinares Formation of La Mola  
579 de Xert has been interpreted as a long-term regressive (highstand) succession  
580 (Malchus et al., 1995).

581 In the central part of the Morella sub-basin (Fig. 1B), in the surroundings  
582 of the city of Morella (*Comarca* of Els Ports), the Villarroya de los Pinares  
583 Formation includes forced regressive, lowstand normal regressive and  
584 highstand normal regressive deposits (Bover-Arnal et al., 2014). In this area,  
585 the highstand platform was thicker than 80 metres, whereas the lowstand  
586 platform and the forced regressive wedge were ca. 10 and 5 m thick,  
587 respectively (Bover-Arnal et al., 2014). On the other hand, in a platform-to-basin  
588 transition found in the Galve sub-basin (western Maestrat Basin; Fig. 1B), the  
589 Villarroya de los Pinares Formation exhibits downlapping slope geometries over  
590 and into the marls of the Forcall Formation, and it is stacked in an aggrading-  
591 retrograding pattern, which indicates a highstand normal regressive unit (Bover-  
592 Arnal et al., 2009, 2012; Gili et al., 2016). The thickness of this highstand  
593 platform where it is wholly preserved is around 50 metres (Bover-Arnal et al.,  
594 2010). Thinner isolated highstand platforms (ca. 15 m thick) and thicker  
595 highstand platform carbonate successions (ca. 90 m thick) belonging to the  
596 Villarroya de los Pinares Formation also occur in the Galve sub-basin (Bover-  
597 Arnal et al., 2010, 2015). In this western marginal part of the Maestrat Basin,  
598 there are also sedimentary bodies belonging to the Villarroya de los Pinares  
599 Formation, which are interpreted as forced regressive, lowstand normal  
600 regressive and transgressive deposits (Bover-Arnal et al., 2009, 2010, 2015).  
601 Interpreted lowstand and forced regressive units belonging to the Villarroya de  
602 los Pinares Formation in the Galve sub-basin are up to 32 and 5 m thick,  
603 respectively (Bover-Arnal et al. 2009; Skelton et al., 2010). Finally, the  
604 highstand platforms cropping out in the Galve sub-basin were subaerially  
605 exposed and incised during the late Early Aptian (Peropadre et al., 2007; Bover-  
606 Arnal et al., 2009, 2010, 2015).

607 On the other hand, in Ulldecona, signs of subaerial exposure at the top of  
608 the Villarroya de los Pinares Formation were not observed, thus this  
609 stratigraphic surface was interpreted as a maximum regressive surface (Figs. 7,  
610 13B-C). However, it could also be that the signs of emersion were masked or  
611 removed by the latest Early Aptian transgression depositing the marls of the  
612 Benassal Formation (Figs. 7, 13A-C). The relatively thick succession exhibited  
613 by the Villarroya de los Pinares Formation in the Grossa Range (ca. 300 m  
614 thick) and the strong aggrading component of its upper part (Fig. 7), which is  
615 typical of inner platform settings, suggests that it was developed during a  
616 highstand normal regressive stage of sea level.

617 Sedimentary records of uppermost lower Aptian regressive platform  
618 carbonates are extensive in coeval basins of the Tethys and the Atlantic  
619 extension of it (e.g., Röhl and Ogg, 1998; Bosellini et al., 1999; Lehmann et al.,  
620 2000; van Buchem et al., 2010; Hfaiedh et al., 2013; Schlagintweit et al., 2016).  
621 In the Arabian Plate for example, the uppermost lower Aptian regressive  
622 limestones characterized by the presence of rudists belong to the Shu'aiba  
623 Formation and are also of economic importance but as hydrocarbon reservoirs  
624 (van Buchem et al., 2010; Yose et al., 2010). Furthermore, as reported from the

625 Galve sub-basin (Fig. 1B; Bover-Arnal et al., 2009, 2010, 2015), carbonate  
626 platforms from different Tethyan locations were also subaerially exposed  
627 around the boundary between the early and the late Aptian (e.g., Arnaud and  
628 Arnaud-Vanneau, 1989; Bernaus et al., 2003; Hillgärtner et al., 2003;  
629 Bachmann and Hirsch, 2006; Husinec and Jelaska, 2006; Yilmaz and Altiner,  
630 2006; Burla et al., 2008; Husinec et al., 2012; Rameil et al., 2012; Fernández-  
631 Mendiola et al., 2013; Ruberti et al., 2013).

632 This widespread late early Aptian low-frequency regression has been  
633 linked to a glacio-eustatic event in some studies (e.g., Bover-Arnal et al., 2009;  
634 Husinec et al., 2012; Rameil et al., 2012; Maurer et al., 2013), and thus to a late  
635 early Aptian cooling episode (Solé de Porta and Salas, 1994; Hochuli et al.,  
636 1999; Steuber et al., 2005; Bover-Arnal et al., 2010; Skelton and Gili, 2012;  
637 Bottini et al., 2015; Cors et al., 2015; Bonin et al., 2016; Pascual-Cebrian et al.,  
638 2016). However, other water sequestration mechanisms such aquifer-eustasy  
639 or changes in the container capacity of the oceans (Immenhauser, 2005;  
640 Cloetingh and Haq, 2015; Sames et al., 2016; Wendler and Wendler, 2016;  
641 Wendler et al., 2016) could have also partly governed these high-rank sea-level  
642 changes identified in Ulldecona.

643 Along the same lines, the marine transgression and regression that led  
644 respectively to the deposition of the marls of the Forcall Formation and the  
645 platform carbonates of the Villarroya de los Pinares Formation in the Grossa  
646 Range during the early Aptian are correlatable with the Tethyan and global  
647 short-term sea-level events Ap3 of Hardenbol et al. (1998) and KAp1 of Haq  
648 (2016). Accordingly, the early Aptian high-rank transgressive-regressive sea-  
649 level trend characterized in the Grossa Range (Fig. 7) was in large part a  
650 eustatic event.

651 Nonetheless, in the Maestrat Basin, the record of the lower Aptian  
652 transgressive marly deposits of the Forcall Formation is slightly diachronous  
653 (Fig. 4; Bover-Arnal et al., 2016). In the Morella and Galve sub-basins (Fig. 1B),  
654 the Forcall Formation spans the four early Aptian ammonoid zones, namely  
655 *Deshayesites oglanlensis*, *Deshayesites forbesi*, *Deshayesites deshayesi* and  
656 *Dufrenoyia furcata* (Garcia et al., 2014; Bover-Arnal et al., 2016), whereas in the  
657 Oliete sub-basin (Fig. 1B), it only spans the *Deshayesites forbesi* Zone  
658 (Moreno-Bedmar et al., 2010; Garcia et al., 2014). Along the same lines, the  
659 regressive platform carbonates of the Villarroya de los Pinares Formation are of  
660 upper lower Aptian age (intra *Dufrenoyia furcata* Zone) in the Morella Sub-basin  
661 and the central Galve Sub-basin (Bover-Arnal et al., 2010, 2014, 2016),  
662 whereas in the eastern part of the Galve Sub-basin it spans the *Deshayesites*  
663 *deshayesi* and *Dufrenoyia furcata* zones (Bover-Arnal et al., 2010, 2016). These  
664 facts highlight that antecedent topography and local to regional tectonics played  
665 a part in controlling accommodation in the Maestrat Basin during the early  
666 Aptian global transgressive-regressive trend.

667 In the Grossa Range, the carbonate platform of the Villarroya de los  
668 Pinares Formation was drowned during the latest early Aptian and buried under

669 transgressive marls of the base of the Benassal Formation (Figs. 7, 13A-C).  
670 Drowning of carbonate platforms during the latest early Aptian or at the early/late  
671 Aptian boundary has been reported from within the Maestrat Basin (Bover-Arnal  
672 et al., 2010, 2014, 2016), but also from geographically distant locations such as  
673 Central Iran (Wilmsen et al., 2013), south-eastern France (Masse and Fenerci-  
674 Masse, 2011), Mexico (Moreno-Bedmar et al., 2012a) or Venezuela (Jacquin et  
675 al., 1993).

676 Above the transgressive marls of the lowermost Benassal Formation  
677 (Figs. 7, 13A), a carbonate platform with mesorbitolinids and rudists belonging  
678 to the lower part of the same formation flourished during an early late Aptian  
679 regression (Figs. 7, 13D). This low-frequency transgressive-regressive sea-level  
680 trend recorded by the lower part of the Benassal Formation and preserved in  
681 Ulldecona is correlatable with the Tethyan and global short-term sea-level  
682 events Ap4 of Hardenbol et al. (1998) and KAp2 of Haq (2016). Consequently,  
683 this additional high-rank transgressive-regressive sequence of latest early-early  
684 late Aptian age (Fig. 7) is interpreted to have been largely controlled by eustasy  
685 as well.

686 Concerning the dolomitized levels studied in Ulldecona (Figs. 7, 14-15),  
687 massive dolomitization of the lower Aptian Villarroya de los Pinares Formation  
688 mainly occurs in eastern parts of the Maestrat Basin including the sub-basins of  
689 Morella, El Perelló, La Salzedella and Penyagolosa (Fig. 1B) (see Salas, 1987;  
690 Nadal, 2001). In addition, throughout the Maestrat Basin, minor saddle dolomite  
691 is also frequently found pore filling in large skeletal components such as rudist  
692 shells and corals of the Villarroya de los Pinares Formation (Bover-Arnal et al.,  
693 2010, 2014). Nevertheless, lower Aptian volumetrically large, replacive  
694 dolostones are poorly studied in the Maestrat Basin (Salas, 1987; Nadal, 2001).  
695 One of these rare studies is that from El Coll del Vidre section (Fig. 1B;  
696 Penyagolosa sub-basin), nearby the town of Vistabella del Maestrat (*Comarca*  
697 of l'Alcalatén), where Nadal (2001) reported the occurrence of massive  
698 dolostones exhibiting a destructive and pervasive fabric with an idiotopic-  
699 hypidiotopic mosaic, as well as widespread saddle dolomite, replacing lower  
700 Aptian limestones. The geometry of this dolomitized geobody belonging to the  
701 Villarroya de los Pinares Formation, however, is not recognizable according to  
702 Nadal (2001).

703 On the other hand, more attention has been paid to dolomitization of  
704 upper Aptian limestones of the Benassal Formation (Nadal, 2011; Martín-Martín  
705 et al., 2013, 2015, 2017; Corbella et al., 2014; Gomez-Rivas et al., 2014). In the  
706 Orpesa Range (Fig. 1B; Penyagolosa sub-basin), to the northeast of the city of  
707 Benicàssim (*Comarca* of La Plana Alta), dolostones belonging to the Benassal  
708 Formation form seismic-scale stratabound tabular geobodies, which are  
709 associated with fault zones and Mississippi Valley Type deposits. Dolostones  
710 from the Orpesa Range are mainly characterized by replacive dolomites with  
711 non-planar textures and saddle dolomite (Martín-Martín et al., 2013, 2015;  
712 Gomez-Rivas et al., 2014). Accordingly, dolomitization in this area has been

713 interpreted as a hydrothermal process (above 80°C), which would have  
714 occurred during the Late Cretaceous post-rift stage of the Maestrat Basin  
715 (Martín-Martín et al., 2013, 2015; Gomez-Rivas et al., 2014). Given the absence  
716 of xenotopic mosaics, saddle dolomite or Mississippi Valley Type ore deposits in  
717 the samples from Ulldecona examined (Fig. 15), the dolomitized interval studied  
718 (Figs. 5, 7, 14) would correspond to a lower-temperature, and perhaps to  
719 different, dolomitization event than the one described in Benicàssim. In this  
720 respect, idiotopic and hypidiotopic mosaic textures such as the ones observed  
721 in Ulldecona (Fig. 15) are commonly linked to temperatures below 50-60°C  
722 during dolomitization (Sibley and Gregg, 1987). Furthermore, in the Grossa  
723 Range it is currently unknown whether or not the dolomitization event  
724 characterized was controlled by faults.

725

## 726 **9. Conclusions**

727

728 The ornamental and building Stone from Ulldecona, commercially known  
729 as 'Sénia stone', corresponds to the Villarroya de los Pinares Formation of the  
730 Maestrat Basin. The Stone from Ulldecona is mainly constituted by limestones,  
731 locally bioturbated, with wackestone, packstone and grainstone textures rich in  
732 peloids, miliolids, orbitolinids, dasycladaceans and bivalves. Given the  
733 occurrence of *Orbitolinopsis simplex* together with *Palorbitolina lenticularis*, the  
734 Stone from Ulldecona is lower Aptian in age. Furthermore, the *Polyconites*  
735 rudists observed exhibit a relatively thick aragonite wall, a flattened left valve,  
736 and a modest size, which are indicative features of specimens of late early  
737 Aptian age (*Dufrenoyia furcata* ammonoid zone).

738 The platform carbonates of the Villarroya de los Pinares Formation  
739 characterized in Ulldecona developed on the northern margin of the Tethys  
740 Ocean in a eustatic regressive context, which post-dated the late Barremian-  
741 early Aptian global transgressive trend that led to the OAE 1a. The analysed  
742 regressive limestones and the underlying transgressive marls of the Forcall  
743 Formation, which crop out locally in the axial zone of an antiform structure, are  
744 interpreted as a large-scale (high-rank, low-frequency) transgressive-regressive  
745 sequence. An overlying long-term transgressive-regressive sequence of latest  
746 early-late Aptian age belonging to the Benassal Formation is locally preserved  
747 in the area examined. This second sequence is also of global significance and  
748 made up of transgressive marls, and regressive platform carbonates containing  
749 orbitolinids and rudists.

750 The middle part of the Villarroya de los Pinares Formation studied was  
751 affected by dolomitization during diagenesis. The decimetre- to tens of metres-  
752 thick dolomitized levels are stratabound, thus indicating a facies control on  
753 dolomitization. Dolomitic limestones, calcitic dolostones and dolostones occur.  
754 Dolostones, which are not extracted as ornamental or building rocks in the  
755 quarries of the area, are sucrose and exhibit vacuolar and cave porosities. Initial  
756 and intermediate stages of dolomitization mainly show idiotopic mosaics, and a

757 destructive and pervasive fabric. Locally, retentive and/or selective fabrics also  
758 occur. Advanced dolomitization stages show a destructive and pervasive fabric  
759 with idiotopic and hypidiotopic mosaics, which have been commonly associated  
760 with temperatures below 50-60°C during dolomitization.

761 Lower Aptian limestones with rudists and orbitolinids are well-known  
762 sedimentary records from many basins worldwide and commercially important  
763 hydrocarbon reservoirs in the Arabian Peninsula (i.e., Shu'aiba Formation). This  
764 study, however, also draws attention to the potential as an ornamental/building  
765 stone of these platform carbonates formed along the margins of the Tethys  
766 during a late early Aptian global regression.

767

## 768 **Acknowledgements**

769

770 This investigation was promoted and partly funded by the Direcció  
771 General d'Energia, Mines i Seguretat Industrial del Departament d'Empresa i  
772 Coneixement de la Generalitat de Catalunya. Additional funding came from the  
773 Grup de Recerca Reconegut per la Generalitat de Catalunya 2017 SGR 824  
774 "Geologia Sedimentària" and the I + D + i research project CGL2015-60805-P  
775 (BIOGEOEVENTS) (MINECO, FEDER, EU). We express our gratitude to the  
776 editor Eduardo Koutsoukos, Felix Schlagintweit, Peter W. Skelton and an  
777 anonymous reviewer who greatly improved the manuscript during the peer  
778 review process. Fernando Castell from Industrial Màrmol Export S.A. (Inmar)  
779 and Francesc Marza from Canteras Ebro S.L. kindly permitted us to work within  
780 the quarries. Enric Pascual-Cebrian, Felix Schlagintweit and Peter W. Skelton  
781 are greatly thanked for identifying several fossil specimens. Juan Diego Martín-  
782 Martín is thanked for discussions on the Aptian dolomitized limestones from the  
783 Maestrat Basin. Ferran Torta Navarro, David Parcerisa, and Carme Fernández  
784 from the Ulldecona Tourism Office, are acknowledged for providing a  
785 bibliography on the Stone from Ulldecona. The staff at the Spanish Olympic  
786 Committee kindly allowed us to take pictures of the building interior.

787

788

## 789 **References**

790 Ajuntament d'Ulldecona (2005). Pedra d'Ulldecona. Catalogue. Ajuntament  
791 d'Ulldecona, 31 pp.

792

793 Arnaud, H., Arnaud-Vanneau, A., Blanc-Alétru, M.-C., Adatte, T., Argot, M.,  
794 Delanoy, G., Thieuloy, J.-P., Vermeulen, J., Virgone, A., Virlouvet, B.,  
795 Wermeille, S., 1998. Répartition stratigraphique des orbitolinidés de la plate-  
796 forme urgonienne subalpine et jurassienne (SE de la France). *Géologie Alpine*  
797 74, 3–89.

798

799 Arnaud, H., Arnaud-Vanneau, A., 1989. Sequences de depot et variations du  
800 niveau relatif de la mer au Barremien et a l'Aptien inferieur dans les massifs  
801 subalpins septentrionaux et le Jura (sud-est de la France). Bulletin de la Société  
802 Géologique de France 5, 651–660.

803

804 Bachmann, M., Hirsch, F., 2006. Lower Cretaceous carbonate platform of the  
805 eastern Levant (Galilee and the Golan Heights): stratigraphy and second-order  
806 sea-level change. Cretaceous Research 27, 487–512.

807

808 Bernaus, J.M., Arnaud-Vanneau, A., Caus, E., 2003. Carbonate platform  
809 sequence stratigraphy in a rapidly subsiding area: the Late Barremian-Early  
810 Aptian of the Organyà basin, Spanish Pyrenees. Sedimentary Geology 159,  
811 177–201.

812

813 Bonin, A., Pucéat, E., Vennin, E., Mattioli, E., Aurell, M., Joachimiski, M.,  
814 Barbarin, N., Laffont, R., 2016. Cool episode and platform demise in the Early  
815 Aptian: New insights on the links between climate and carbonate production,  
816 Paleocyanography 31, 66–80. doi:10.1002/2015PA002835.

817

818 Bosellini, A., Russo, A., Schroeder, R., 1999. Stratigraphic evidence for an  
819 Early Aptian sea-level fluctuation: the Graua Limestone of south-eastern  
820 Ethiopia. Cretaceous Research 20, 783-791.

821

822 Bottini, C., Erba, E., Tiraboschi, D., Jenkyns, H.C., Schouten, S., Sinninghe  
823 Damsté, J.S., 2015. Climate variability and ocean fertility during the Aptian  
824 Stage. Climate of the Past 11, 383-402.

825

826 Bover-Arnal, T., Salas, R., Moreno-Bedmar, J.A., Bitzer, K., 2009. Sequence  
827 stratigraphy and architecture of a late Early-Middle Aptian carbonate platform  
828 succession from the western Maestrat Basin (Iberian Chain, Spain).  
829 Sedimentary Geology 219, 280–301.

830

831 Bover-Arnal, T., Moreno-Bedmar, J.A., Salas, R., Skelton, P.W., Bitzer, K., Gili,  
832 E., 2010. Sedimentary evolution of an Aptian syn-rift carbonate system  
833 (Maestrat Basin, E Spain): effects of accommodation and environmental  
834 change. *Geologica Acta* 8, 249–280.

835

836 Bover-Arnal, T., Salas, R., Martín-Closas, C., Schlagintweit, F., Moreno-  
837 Bedmar, J.A., 2011. Expression of an oceanic anoxic event in a neritic setting:  
838 Lower Aptian coral rubble deposits from the western Maestrat Basin (Iberian  
839 Chain, Spain). *Palaios* 26, 18–32.

840

841 Bover-Arnal, T., Löser, H., Moreno-Bedmar, J.A., Salas, R., Strasser, A., 2012.  
842 Corals on the slope (Aptian, Maestrat Basin, Spain). *Cretaceous Research* 37,  
843 43–64.

844

845 Bover-Arnal, T., Salas, R., Guimerà, J., Moreno-Bedmar, J.A., 2014. Deep  
846 incision on an Aptian carbonate succession indicates major sea-level fall in the  
847 Cretaceous. *Sedimentology* 61, 1558–1593.

848

849 Bover-Arnal, T., Pascual-Cebrian, E., Skelton, P.W., Gili, E., Salas, R., 2015.  
850 Patterns in the distribution of Aptian rudists and corals within a sequence-  
851 stratigraphic framework (Maestrat Basin, E Spain). *Sedimentary Geology* 321,  
852 86–104.

853

854 Bover-Arnal, T., Moreno-Bedmar, J.A., Frijia, G., Pascual-Cebrian, E., Salas,  
855 R., 2016. Chronostratigraphy of the Barremian-Early Albian of the Maestrat  
856 Basin (E Iberian Peninsula): integrating strontium-isotope stratigraphy and  
857 ammonoid biostratigraphy. *Newsletters on Stratigraphy* 49, 41–68.

858

859 Burla, S., Heimhofer, U., Hochuli, P.A., Weissert, H., Skelton, P., 2008.  
860 Changes in sedimentary patterns of coastal and deep-sea successions from the  
861 North Atlantic (Portugal) linked to Early Cretaceous environmental change.  
862 *Palaeogeography, Palaeoclimatology, Palaeoecology* 257, 38–57.

863

864 Canérot, J., Cugny, P., Pardo, G., Salas, R., Villena, J., 1982. Ibérica Central-  
865 Maestrazgo. In: García, A. (Ed.), El Cretácico de España. Universidad  
866 Complutense de Madrid, 273–344.

867

868 Castro, J.M., de Gea, G.A., Ruiz-Ortiz, P.A., Nieto, L.M., 2008. Development of  
869 carbonate platforms on an extensional (rifted) margin: the Valanginian-Albian  
870 record of the Prebetic of Alicante (SE Spain). *Cretaceous Research* 29, 848–  
871 860.

872

873 Catuneanu, O., Galloway, W.E., Kendall, C.G.St.C., Miall, A.D., Posamentier,  
874 H.W., Strasser, A., Tucker, M.E., 2011. Sequence stratigraphy: methodology  
875 and nomenclature. *Newsletters on Stratigraphy* 44/3, 173–245.

876

877 Cherchi, A., Schroeder, R., 2013. The *Praeorbitolina/Palorbitolinoides*  
878 Association: an Aptian biostratigraphic key-interval at the southern margin of the  
879 Neo-Tethys. *Cretaceous Research* 39, 70–77.

880

881 Cloetingh, S., Haq, B.U., 2015. Inherited landscapes and sea level change.  
882 *Science* 347, 1258375.

883

884 Cooper, M.R., 1977. Eustacy during the Cretaceous: its implications and  
885 importance. *Palaeogeography, Palaeoclimatology, Palaeoecology* 22, 1–60.

886

887 Corbella, M., Gomez-Rivas, E., Martín-Martín, J.D., Stafford, S.L., Teixell, A.,  
888 Griera, A., Travé, A., Cardellach, E., Salas, R., 2014. Insights to controls on  
889 dolomitization by means of reactive transport models applied to the Benicàssim  
890 case study (Maestrat Basin, eastern Spain). *Petroleum Geoscience* 20, 41–54.

891

892 Cors, J., Heimhofer, U., Adatte, T., Hochuli, P.A., Huck, S., Bover-Arnal, T.,  
893 2015. Spore-pollen assemblages show delayed terrestrial cooling in the  
894 aftermath of OAE 1a. *Geological Magazine* 152, 632–647.

895

896 Dunham, R.J., 1962. Classification of carbonate rocks according to depositional  
897 texture. In: Ham, E.R. (Ed.), Classification of carbonate rocks. Am. Assoc.  
898 Petrol. Geol. Mem. 1, 108–121.

899

900 Embry, A.F., Klovan, J.E., 1971. A Late Devonian reef tract on northeastern  
901 Banks Island, N.W.T. Bulletin of Canadian Petroleum Geology 19, 730–781.

902

903 Embry, J.-C., Vennin, E., Van Buchem, F. S. P., Schroeder, R., Pierre, C.,  
904 Aurell, M., 2010. Sequence stratigraphy and carbon isotope stratigraphy of an  
905 Aptian mixed carbonate-siliciclastic platform to basin transition (Galve sub-  
906 basin, NE Spain). In: Van Buchem, F. S. P., Gerdes, K. D., Esteban, M. (Eds.),  
907 Mesozoic and Cenozoic Carbonate Systems of the Mediterranean and the  
908 Middle East: Stratigraphic and Diagenetic Reference Models. Geological  
909 Society Special Publications, London 329, 113–143.

910

911 Fernández Burriel, D., 2009. Caracterització de les calcàries explotables com a  
912 roca ornamental al Montsià (Unpubl. Degree thesis). Escola Politècnica  
913 Superior d'Enginyeria de Manresa, Universitat Politècnica de Catalunya, 40 pp.  
914 (available at <http://hdl.handle.net/2117/116918>).

915

916 Fernández, D., Parcerisa, D., Alfonso, M. P., Cobo, A., 2009. Caracterización y  
917 valor patrimonial de la Pedra de Ulldecona (Montsià). In: X Congreso  
918 Internacional sobre Patrimonio Geológico y Minero, Instituto Geológico y Minero  
919 de España, 32–33.

920

921 Fernández-Mendiola, P.A., Mendicoa, J., Hernandez, S., Owen, H.G., García-  
922 Mondéjar, J., 2013. A facies model for an Early Aptian carbonate platform  
923 (Zamaia, Spain). *Facies* 59, 529–558.

924

925 Fernández-Mendiola, P.A., Mendicoa, J., Owen, H.G., García-Mondéjar, J.,  
926 2017. The Early Aptian (Cretaceous) stratigraphy of Mount Pagasarri (N Spain):  
927 Oceanic anoxic event-1a. *Geological Journal* 53, 1802–1822.

928

929 Föllmi, K.B., Weissert, H., Bisping, M., Funk, H., 1994. Phosphogenesis,  
930 carbon-isotope stratigraphy, and carbonate-platform evolution along the Lower

931 Cretaceous northern Tethyan margin. Geological Society of America Bulletin  
932 106, 729–746.

933

934 Garcia, R., Moreno-Bedmar, J.A., Bover-Arnal, T., Company, M., Salas, R.,  
935 Latil, J.L., Martín-Martín, J.D., Gomez-Rivas, E., Bulot, L.G., Delanoy, G.,  
936 Martínez, R., Grauges, A., 2014. Lower Cretaceous (Hauterivian-Albian)  
937 ammonite biostratigraphy in the Maestrat Basin (E Spain). Journal of Iberian  
938 Geology 40, 99–112.

939

940 García-Mondéjar, J., Owen, H.G., Raisossadat, N., Millán, M.I., Fernández-  
941 Mendiola, P.A., 2009. The Early Aptian of Aralar (northern Spain): stratigraphy,  
942 sedimentology, ammonite biozonation, and OAE1. Cretaceous Research 30,  
943 434–464.

944

945 Gili, E., Skelton, P.W., Bover-Arnal, T., Salas, R., Obrador, A., Fenerci-Masse,  
946 M., 2016. Depositional biofacies model for post-OAE1a Aptian carbonate  
947 platforms of the western Maestrat Basin (Iberian Chain, Spain).  
948 Palaeogeography, Palaeoclimatology, Palaeoecology 453, 101–114.

949

950 Gomez-Rivas, E., Corbella, M., Martín-Martín, J.D., Stafford, S.L., Teixell, A.,  
951 Bons, P.D., Griera, A., Cardellach, E., 2014. Reactivity of dolomitizing fluids and  
952 Mg source evaluation of fault- controlled dolomitization at the Benicàssim  
953 outcrop analogue (Maestrat basin, E Spain). Marine and Petroleum Geology 55,  
954 26–42.

955

956 Gradstein, F.M., Ogg, J.G., Smith, A.G., 2004. A Geologic Time Scale 2004.  
957 Cambridge University Press, Cambridge, 610 pp.

958

959 Granier, B., Clavel, B., Moullade, M., Busnardo, R., Charollais, J., Tronchetti,  
960 G., Desjacques P., 2013. L'Estellon (Baronnies, France), a "Rosetta Stone" for  
961 the Urgonian biostratigraphy. Carnets de Géologie [Notebooks on Geology],  
962 Article 2013/04 (CG2013\_A04), 163–207.

963

964 Grauges, A., Moreno-Bedmar, J.A., Martínez, R., 2010. Desmocerátidos  
965 (Ammonoidea) del Aptiense Inferior (Cretácico Inferior) de la subcuena de

- 966 Oliete, Cordillera Ibérica Oriental (Teruel, España). *Revista Española de*  
967 *Paleontología* 25, 7–18.
- 968
- 969 Haq, B.U., 2014. Cretaceous eustasy revisited. *Global and Planetary Change*  
970 113, 44–58.
- 971
- 972 Hardenbol, J., Thierry, J., Farley, M.B., Jacquin, T., Graciansky, de P.-C., Vail,  
973 P.R., 1998. Mesozoic and Cenozoic sequence chronostratigraphic framework of  
974 European basins. In: Graciansky, de P.-C., Hardenbol, J., Jacquin, T., Vail, P.R.  
975 (Eds.), *Mesozoic and Cenozoic sequence stratigraphy of European basins*.  
976 SEPM Special Publication 60, 3–13.
- 977
- 978 Hillgärtner, H., van Buchem, F.S.P., Gaumet, F., Razin, P., Pittet, B., Grötsch,  
979 J., Droste, H., 2003. The Barremian-Aptian evolution of the eastern Arabian  
980 carbonate platform margin (northern Oman). *Journal of Sedimentary Research*  
981 73, 3–13.
- 982
- 983 Hfaiedh, R., Arnaud Vanneau, A., Godet, A., Arnaud, H., Zghal, I., Ouali, J.,  
984 Latil, J.-L., Jallali, H., 2013. Biostratigraphy, palaeoenvironments and sequence  
985 stratigraphy of the Aptian sedimentary succession at Jebel Bir Oum Ali  
986 (Northern Chain of Chotts, South Tunisia): Comparison with contemporaneous  
987 Tethyan series. *Cretaceous Research* 46, 177–207.
- 988
- 989 Hochuli, P.A., Menegatti, A.P., Weissert, H., Riva, A., Erba, E., Premoli Silva, I.,  
990 1999. Episodes of high productivity and cooling in the early Aptian Alpine  
991 Tethys. *Geology* 27, 657–660.
- 992
- 993 Husinec, A., Jelaska, V., 2006. Relative sea-level changes recorded on an  
994 isolated carbonate platform: Tithonian to Cenomanian succession, Southern  
995 Croatia. *Journal of Sedimentary Research* 76, 1120–1136.
- 996
- 997 Husinec, A., Harman, C.A., Regan, S.P., Mosher, D.A., Sweeney, R.J., Read,  
998 J.F., 2012. Sequence development influenced by intermittent cooling events in  
999 the Cretaceous Aptian greenhouse, Adriatic platform, Croatia. *AAPG Bulletin*  
1000 96, 2215–2244.

1001

1002 Immenhauser, A., 2005. High-rate sea-level change during the Mesozoic: New  
1003 approaches to an old problem. *Sedimentary Geology* 175, 277–296.

1004

1005 Jacquin, T., Azpirixaga, I., Murat, B., Roberto, M.F., 1993. Sequential evolution  
1006 of Lower Cretaceous carbonate platforms in the Maracaibo Basin, Venezuela.  
1007 *American Association of Petroleum Geologists Bulletin* 77, pp. 326.

1008

1009 Johnson, J. G., Murphy, M. A., 1984. Time-rock model for Siluro-Devonian  
1010 continental shelf, western United States. *Geological Society of America Bulletin*  
1011 95, 1349–1359.

1012

1013 Lehmann, C., Osleger, D.A., Montañez, I., 2000. Sequence stratigraphy of  
1014 Lower Cretaceous (Barremian-Albian) carbonate platforms of northeastern  
1015 Mexico: regional and global correlations. *Journal of Sedimentary Research* 70,  
1016 373–391.

1017

1018 Lehmann, J., Maisch, M.W., Baudouin, C., Salfinger-Maisch, A., 2017. Origin  
1019 and evolutionary history of *Anglonautilus* (Nautilida, Cymatoceratidae) and a  
1020 new species from the lower Aptian of Spain. *Cretaceous Research* 72, 66–80.

1021

1022 Leyva, F., Martín, L., Canérot, J., 1972. Ulldecona, hoja nº 546. Mapa  
1023 Geológico de España 1:50.000. 2ª Serie. 1ª Edición. Servicio de Publicaciones,  
1024 Ministerio de Industria y Energía, Madrid, 20 pp.

1025

1026 Malchus, N., Pons, J.M., Salas, R., 1995. Rudist distribution in the Lower Aptian  
1027 shallow platform of La Mola de Xert, eastern Iberian Range, NE Spain. *Revista*  
1028 *Mexicana de Ciencias Geológicas* 12, 224–235.

1029

1030 Martín, J.D., Sanfeliu, T., Ovejero, M., de la Fuente, C., 2001. La piedra natural  
1031 en la provincia de Castellón. *Roc Maquina* 66, 36–40.

1032

- 1033 Martín-Martín, J.D., Gomez-Rivas, E., Bover-Arnal, T., Travé, A., Salas, R.,  
1034 Moreno-Bedmar, J.A., Tomás, S., Corbella, M., Teixell, A., Vergés, J., Stafford,  
1035 S.L., 2013. The Upper Aptian to Lower Albian synrift carbonate succession of  
1036 the southern Maestrat Basin (Spain): Facies architecture and fault-controlled  
1037 stratabound dolostones. *Cretaceous Research* 41, 217–236.
- 1038
- 1039 Martín-Martín, J.D., Travé, A., Gomez-Rivas, E., Salas, R., Sizun, J.-P., Vergés,  
1040 J., Corbella, M., Stafford, S.L., Alfonso, P., 2015. Fault-controlled and  
1041 stratabound dolostones in the Late Aptian-earliest Albian Benassal Formation  
1042 (Maestrat Basin, E Spain): Petrology and geochemistry constrains. *Marine and  
1043 Petroleum Geology* 65, 83–102.
- 1044
- 1045 Martín-Martín, J.D., Gomez-Rivas, E., Gómez-Gras, D., Travé, A., Ameneiro,  
1046 R., Koehn, D., Bons, P.D., 2017. Activation of stylolites as conduits for  
1047 overpressured fluid flow in dolomitized platform carbonates. *Geological Society,  
1048 London, Special Publications* 459, <https://doi.org/10.1144/SP459.3>
- 1049
- 1050 Martínez, R., Grauges, A., 2006. Nautilídeos del Aptiense Inferior (Cretácico  
1051 inferior) de la Subcuenca de Oliete, Cordillera Ibérica Oriental (Teruel, España).  
1052 *Revista Española de Paleontología* 21, 15–27.
- 1053
- 1054 Mas, R., 1981. El Cretácico inferior de la región noroccidental de la provincia de  
1055 Valencia (Unpubl. PhD thesis). Universidad Complutense de Madrid, 409 pp.
- 1056
- 1057 Masse, J.P., 2003. Integrated stratigraphy of the Lower Aptian and applications  
1058 to carbonate platforms: a state of the art. In: Gili E., Negra, M., Skelton, P.W.  
1059 (Eds.), *North African Cretaceous Carbonate Platform Systems*. Kluwer  
1060 Academic Publishers, 203–214.
- 1061
- 1062 Masse, J.-P., Fenerci-Masse, M., 2011. Drowning discontinuities and  
1063 stratigraphic correlation in platform carbonates. The late Barremian-early Aptian  
1064 record of southeast France. *Cretaceous Research* 32, 659–684.
- 1065

- 1066 Maurer, F., van Buchem, F.S.P., Eberli, G.P., Pierson, B.J., Raven, M.J.,  
1067 Larsen, P.-H., Al-Husseini, M.I., Benoit, V., 2013. Late Aptian long-lived glacio-  
1068 eustatic lowstand recorded on the Arabian Plate. *Terra Nova* 25, 87-94.
- 1069
- 1070 Moreno-Bedmar, J.A., Bulot, L.G., Latil, J.-L., Martínez, R., Ferrer, O. Bover-  
1071 Arnal, T., Salas, R., 2008. Precisiones sobre la edad de la base de la Fm.  
1072 Escucha, mediante ammonioideos, en la subcuena de la Salzedella, Cuenca  
1073 del Maestrat (E Cordillera Ibérica). *Geo-Temas* 10, 1260–1272.
- 1074
- 1075 Moreno-Bedmar, J.A., Garcia, R., 2011. Análisis bioestratigráfico de los  
1076 ammonioideos del Aptiense inferior (Cretácico Inferior) del Miembro Cap de  
1077 Vinyet (Foramción Margas del Forcall) de la subcuena de Morella (Castellón).  
1078 In: Pérez-García, A., Gascó, F., Gasulla, J.M., Escaso, F. (Eds.), *Viajando a*  
1079 *Mundos Pretéritos*. Ayuntamiento de Morella, Morella, Castellón, 215–222.
- 1080
- 1081 Moreno-Bedmar, J.A., Company, M., Bover-Arnal, T., Salas, R., Delanoy, G.,  
1082 Martínez, R., Grauges, A., 2009. Biostratigraphic characterization by means of  
1083 ammonoids of the lower Aptian Oceanic Anoxic Event (OAE1a) in the eastern  
1084 Iberian Chain (Maestrat Basin, eastern Spain). *Cretaceous Research* 30, 864–  
1085 872.
- 1086
- 1087 Moreno-Bedmar, J.A., Company, M., Bover-Arnal, T., Salas, R., Maurrasse,  
1088 F.J., Delanoy, G., Grauges, A., Martínez, R., 2010. Lower Aptian ammonite  
1089 biostratigraphy in the Maestrat Basin (Eastern Iberian Chain, Eastern Spain). *A*  
1090 *Tethyan transgressive record enhanced by synrift subsidence*. *Geologica Acta*  
1091 8, 281–299.
- 1092
- 1093 Moreno-Bedmar, J.A., Bover-Arnal, T., Barragán, R., Salas, R., 2012a.  
1094 Uppermost Lower Aptian transgressive records in Mexico and Spain:  
1095 chronostratigraphic implications for the Tethyan sequences. *Terra Nova* 24,  
1096 333–338.
- 1097
- 1098 Moreno-Bedmar, J.A., Company, M., Sandoval, J., Tavera, J.M., Bover-Arnal,  
1099 T., Salas, R., Delanoy, G., Maurrasse, F.J.-M.R., Martínez, R., 2012b. Lower  
1100 Aptian ammonite and carbon isotope stratigraphy in the eastern Prebetic  
1101 Domain (Betic Cordillera, southeastern Spain). *Geologica Acta* 4, 333–350.

1102

1103 Moreno-Bedmar, J.A., Barragán, R., Delanoy, G., Company, M., Salas, R.,  
1104 2014. Review of the early Aptian (Early Cretaceous) ammonoid species  
1105 *Deshayesites deshayesi* (d'Orbigny, 1841). *Cretaceous Research* 51, 341–360.

1106

1107 Moreno-Bedmar, J.A., Albalat, D., Mallofré, A., Ossó, À., Vilà, M., 2016.  
1108 Estratigrafia mesozoica i nous cefalòpodes de l'Aptià del Vendrell, sud-oest del  
1109 massís del Garraf (Catalunya). *Nemus* 6, 61-72.

1110

1111 Nadal, J., 2001. Estudi de la dolomitització del Juràssic superior-Cretaci inferior  
1112 de la Cadena Ibèrica oriental i la Cadena Costanera Catalana: relació amb la  
1113 segona etapa de rift mesozoica. Unpublished PhD thesis, Universitat de  
1114 Barcelona, 447 pp.

1115

1116 Nebot, M., Guimerà, J., 2016. Structure of an inverted basin from subsurface  
1117 and field data: the Late Jurassic-Early Cretaceous Maestrat Basin (Iberian  
1118 Chain). *Geologica Acta* 14, 155–177.

1119

1120 Nebot, M., Guimerà, J., 2018. Kinematic evolution of a fold-and-thrust belt  
1121 developed during basin inversion: the Mesozoic Maestrat basin, E Iberian  
1122 Chain. *Geological Magazine* 155, 630–640.

1123

1124 Ossó, À., van Bakel, B., Ferratges-Kwekel, F.A., Moreno-Bedmar, J.A., 2018. A  
1125 new decapod crustacean assemblage from the lower Aptian of La Cova del  
1126 Vidre (Baix Ebre, province of Tarragona, Catalonia). *Cretaceous Research* 92,  
1127 94-107.

1128

1129 Pascual-Cebrian, E., 2014. Shell evolution of the Polyconitidae during the  
1130 Aptian of Iberia: A grinding tomography method to map calcite/aragonite  
1131 fluctuations in rudist bivalves (Unpubl. PhD thesis). Universität Heidelberg, 144  
1132 pp.

1133

- 1134 Pascual-Cebrian, E., Götz, S., Bover-Arnal, T., Skelton, P.W., Gili, E., Salas, R.,  
1135 Stinnesbeck, W., 2016. Calcite/aragonite ratio fluctuations in Aptian rudist  
1136 bivalves: Correlation with changing temperatures. *Geology* 44, 135–138.
- 1137
- 1138 Peropadre, C., Meléndez, N., Liesa, C.L., 2007. A 60 metres Aptian sea-level  
1139 fall from the Galve sub-basin (Eastern Spain). 25th IAS Meeting of  
1140 Sedimentology, abstract vol., Patras, Greece, September 2007, pp. 27.
- 1141
- 1142 Pictet, A., Delanoy, G., Adatte, T., Spangenberg, J.E., Baudouin, C., Boselli, P.,  
1143 Boselli, M., Kindler, P., Föllmi, K.B., 2015. Three successive phases of platform  
1144 demise during the early Aptian and their association with the oceanic anoxic  
1145 Selli episode (Ardèche, France). *Palaeogeography, Palaeoclimatology,*  
1146 *Palaeoecology* 418, 101–125.
- 1147
- 1148 Pittet, B., Van Buchem, F.S.P., Hillgärtner, H., Razin, P., Grötsch, J., Droste, H.,  
1149 2002. Ecological succession, palaeoenvironmental change, and depositional  
1150 sequences of Barremian-Aptian shallow-water carbonates in northern Oman.  
1151 *Sedimentology* 49, 555–581.
- 1152
- 1153 Posenato, R., Morsilli, M., Guerzoni, S., Bassi, D., 2018. Palaeoecology of  
1154 *Chondrodonta* (Bivalvia) from the lower Aptian (Cretaceous) Apulia Carbonate  
1155 Platform (Gargano Promontory, southern Italy). *Palaeogeography,*  
1156 *Palaeoclimatology, Palaeoecology* 508, 188–201.
- 1157
- 1158 Rameil, N., Immenhauser, A., Csoma, A. É., Warrlich, G., 2012. Surfaces with a  
1159 long history: the Aptian top Shu'aiba Formation unconformity, Sultanate of  
1160 Oman. *Sedimentology* 59, 212–248.
- 1161
- 1162 Röhl, U., Ogg, J.G., 1998. Aptian-Albian eustatic sea-levels. In: Reefs and  
1163 carbonate platforms in the Pacific and Indian oceans. (Eds. G.F. Camoin and  
1164 P.J. Davies). IAS Special Publication 25, 95–136.
- 1165
- 1166 Ruberti, D., Bravi, S., Carannante, G., Vigorito, M., Simone, L., 2013. Decline  
1167 and recovery of the Aptian carbonate factory in the southern Apennine

- 1168 carbonate shelves (southern Italy): Climatic/oceanographic vs. local tectonic  
1169 controls. *Cretaceous Research* 39, 112–132.
- 1170
- 1171 Sahagian, D., Pinous, O., Olfieriev, A., Zakharov, V., 1996. Eustatic curve for  
1172 the Middle Jurassic-Cretaceous based on Russian Platform and Siberian  
1173 stratigraphy: zonal resolution. *AAPG Bulletin* 80, 1433–1458.
- 1174
- 1175 Salas, R., 1987. El Malm i el Cretaci inferior entre el Massís de Garraf i la Serra  
1176 d'Espadà. Anàlisi de Conca (Unpubl. PhD thesis), Universitat de Barcelona, 345  
1177 pp.
- 1178
- 1179 Salas, R., Casas, A., 1993. Mesozoic extensional tectonics, stratigraphy, and  
1180 crustal evolution during the Alpine cycle of the eastern Iberian basin.  
1181 *Tectonophysics* 228, 33–55.
- 1182
- 1183 Salas, R., Martín-Closas, C., Querol, X., Guimerà, J., Roca, E., 1995. Evolución  
1184 tectonosedimentaria de las cuencas del Maestrazgo y Aliaga-Penyagolosa  
1185 durante el Cretácico inferior. In: Salas, R., Martín-Closas, C. (Eds.), *El*  
1186 *Cretácico inferior del Nordeste de Iberia*. Barcelona, Universitat de Barcelona,  
1187 13–94.
- 1188
- 1189 Salas, R., Guimerà, J., 1996. Rasgos estructurales principales de la cuenca  
1190 Cretácica Inferior del Maestrazgo (Cordillera Ibérica oriental). *Geogaceta* 20,  
1191 1704–1706.
- 1192
- 1193 Salas, R., Guimerà, J., Mas, R., Martín-Closas, C., Meléndez, A., Alonso, A.,  
1194 2001. Evolution of the Mesozoic Central Iberian Rift System and its Cainozoic  
1195 inversion (Iberian Chain). In: Ziegler, P.A., Cavazza, W., Roberston, A.H.F.,  
1196 Crasquin-Soleau, S. (Eds.), *Peri-Tethys Memoir 6: Peri-Tethyan Rift/Wrench*  
1197 *Basins and Passive Margins. Mémoires du Muséum National d'Histoire*  
1198 *Naturelle, Paris* 186, 145–186.
- 1199
- 1200 Sames, B., Wagreeich, M., Wendler, J.E., Haq, B.U., Conrad, C.P., Melinte-  
1201 Dobrinescu, M.C., Hu, X., Wendler, I., Wolfgring, E., Yilmaz, I.Ö., Zorina, S.O.,  
1202 2016. Review: Short-term sea-level changes in a greenhouse world – A view

- 1203 from the Cretaceous. *Palaeogeography, Palaeoclimatology, Palaeoecology*  
1204 441, 393–411.
- 1205
- 1206 Sanchez-Hernandez, Y., Maurrasse, F.J.-M.R., Melinte-Dobrinescu, M.C., He,  
1207 D., Butler, S.K., 2014. Assessing the factors controlling high sedimentation  
1208 rates from the latest Barremian–earliest Aptian in the hemipelagic setting of the  
1209 restricted Organyà Basin, NE Spain. *Cretaceous Research* 51, 1–21.
- 1210
- 1211 Schlagintweit, F., Bover-Arnal, T., Salas, R., 2010. Erratum to: New insights into  
1212 *Lithocodium aggregatum* Elliott 1956 and *Bacinella irregularis* Radoičić 1959  
1213 (Late Jurassic-Lower Cretaceous): two ulvophycean green algae (?Order  
1214 Ulotrichales) with a heteromorphic life cycle (epilithic/euendolithic). *Facies* 56,  
1215 635–673.
- 1216
- 1217 Schlagintweit, F., Bover-Arnal, T., 2012. The morphological adaption of  
1218 *Lithocodium aggregatum* Elliott (calcareous green alga) to cryptic microhabitats  
1219 (Lower Aptian, Spain): an example of phenotypic plasticity. *Facies* 58, 37–55.
- 1220
- 1221 Schlagintweit, F., Bucur, I.I., Rashidi, K., Saberzadeh, B., 2013. *Praeorbitolina*  
1222 *claveli* n. sp. (benthic Foraminifera) from the Lower Aptian *sensu lato*  
1223 (Bedoulian) of Central Iran. *Carnets de Géologie [Notebooks on Geology]*,  
1224 Letter 2013/04 (CG2013\_L04), 255–272.
- 1225
- 1226 Schlagintweit, F., Rosales, I., Najarro, M., 2016. *Glomospirella cantabrica* n.  
1227 sp., and other benthic foraminifera from Lower Cretaceous Urgonian-type  
1228 carbonates of Cantabria, Spain: Biostratigraphic implications. *Geologica Acta*  
1229 14, 113–138.
- 1230
- 1231 Schroeder, R., van Buchem, F.S.P., Cherchi, A., Baghbani, D., Vincent, B.,  
1232 Immenhauser, A., Granier, B. (2010). Revised orbitolinid biostratigraphic  
1233 zonation for the Barremian – Aptian of the eastern Arabian Plate and  
1234 implications for regional stratigraphic correlations. In: van Buchem, F.S.P., Al-  
1235 Hussein, M.I., Maurer, F., Droste, H.J. (Eds.), *Barremian – Aptian Stratigraphy*  
1236 *and Hydrocarbon Habitat of the Eastern Arabian Plate*. *GeoArabia Special*  
1237 *Publication 4, Gulf PetroLink, Bahrain* 1, 49–96.
- 1238

- 1239 Sibley, D.F., Gregg, J.M., 1987. Classification of dolomite rock textures. *Journal*  
1240 *of Sedimentary Petrology* 57, 967–975.
- 1241
- 1242 Skelton, P.W., 2003. Rudist evolution and extinction – a north African  
1243 perspective. In: Gili, E., Negra, M., Skelton, P.W. (Eds.), *North African*  
1244 *Cretaceous Carbonate Platform Systems*. NATO Science Series IV. Earth and  
1245 *Environmental Sciences*, Kluwer Academic Publishers 28, 215–227.
- 1246
- 1247 Skelton, P.W., Gili, E., 2012. Rudists and carbonate platforms in the Aptian: a  
1248 case study on biotic interactions with ocean chemistry and climate.  
1249 *Sedimentology* 59, 81–117.
- 1250
- 1251 Skelton, P.W., Gili, E., Bover-Arnal, T., Salas, R., Moreno-Bedmar, J.A., 2010.  
1252 A new species of Polyconites from the uppermost Lower Aptian of Iberia and  
1253 the early evolution of polyconitid rudists. *Turkish Journal of Earth Sciences* 19,  
1254 557–572.
- 1255
- 1256 Solé de Porta, N., Salas, R., 1994. Conjuntos microflorísticos del Cretácico  
1257 inferior de la Cuenca del Maestrazgo. Cordillera Ibérica Oriental (NE de  
1258 España). *Cuadernos de Geología Ibérica* 18, 355–368.
- 1259
- 1260 Steuber, T., Rauch, M., Masse, J.-P., Graaf, J., Malkoc, M., 2005. Low-latitude  
1261 seasonality of Cretaceous temperatures in warm and cold episodes. *Nature*  
1262 437, 1341–1344.
- 1263
- 1264 Steuber, T., Scott, R. W., Mitchell, S. F., Skelton, P. W., 2016. Part N, Revised,  
1265 Volume 1, Chapter 26C: Stratigraphy and diversity dynamics of Jurassic–  
1266 Cretaceous Hippuritida (rudist bivalves). *Treatise Online* 81, 1–17.
- 1267
- 1268 Suarez-Gonzalez, P., Quijada, I.E., Benito, M.I., Mas, R., 2013. Eustatic *versus*  
1269 tectonic control in an intraplate rift basin (Leza Fm, Cameros Basin).  
1270 Chronostratigraphic and paleogeographic implications for the Aptian of Iberia.  
1271 *Journal of Iberian Geology* 39, 285–312.
- 1272

- 1273 Torta Navarro, F., 2002. La pedra d'Ulldecona: Recerca i patologia. Col·legi  
1274 d'Aparelladors i Arquitectes Tècnics de les Terres de l'Ebre, 94 pp.
- 1275
- 1276 Torta Navarro, F., 2006. La pedra d'Ulldecona a l'obra. Col·legi d'Aparelladors i  
1277 Arquitectes Tècnics de les Terres de l'Ebre, 88 pp.
- 1278
- 1279 van Buchem, F.S.P., Al-Husseini, M.I., Maurer, F., Droste, H.J., Yose, L.A.,  
1280 2010. Sequence-stratigraphic synthesis of the Barremian – Aptian of the  
1281 eastern Arabian Plate and implications for the petroleum habitat. In: Barremian  
1282 – Aptian Stratigraphy and Hydrocarbon Habitat of the Eastern Arabian Plate  
1283 (Eds F.S.P. van Buchem, M.I. Al-Husseini, F. Maurer and H.J. Droste).  
1284 GeoArabia Special Publication 4, Gulf PetroLink, Bahrain, 1, 9–48.
- 1285
- 1286 Vennin, E., Aurell, M., 2001. Stratigraphie séquentielle de l'Aptien du sous-  
1287 bassin de Galvé (Province de Teruel, NE de l'Espagne). Bulletin de la Société  
1288 Géologique de France 172, 397–410.
- 1289
- 1290 Vilas, L., Masse, J.P., Arias, C., 1995. *Orbitolina* episodes in carbonate platform  
1291 evolution: the early Aptian model from SE Spain. Palaeogeography,  
1292 Palaeoclimatology, Palaeoecology 119, 35–45.
- 1293
- 1294 Weisser, D., 1959. Acerca de la estratigrafía del Urgo-Aptense en las cadenas  
1295 Celtibéricas de España. Notas y comunicaciones del Instituto Geológico y  
1296 Minero de España 55, 17–32.
- 1297
- 1298 Wendler, J.E., Wendler, I., 2016. What drove sea-level fluctuations during the  
1299 mid-Cretaceous greenhouse climate? Palaeogeography, Palaeoclimatology,  
1300 Palaeoecology 441, 412–419.
- 1301
- 1302 Wendler, J.E., Wendler, I., Vogt, C., Kuss, J., 2016. Link between cyclic eustatic  
1303 sea-level change and continental weathering: Evidence for aquifer-eustasy in  
1304 the Cretaceous. Palaeogeography, Palaeoclimatology, Palaeoecology 441,  
1305 430–437.
- 1306

- 1307 Wilmsen, M., Fürsich, F.T., Majidifard, M.R., 2015. An overview of the  
1308 Cretaceous stratigraphy and facies development of the Yazd Block, western  
1309 Central Iran. *Journal of Asian Earth Sciences* 102, 73–91.
- 1310
- 1311 Wissler, L., Funk, H., Weissert, H., 2003. Response of Early Cretaceous  
1312 carbonate platforms to changes in atmospheric carbon dioxide levels.  
1313 *Palaeogeography, Palaeoclimatology, Palaeoecology* 200, 187–205.
- 1314
- 1315 Yilmaz, I.Ö., Altiner, D., 2006. Cyclic palaeokarst surfaces in Aptian peritidal  
1316 carbonate successions (Taurides, southwest Turkey): internal structure and  
1317 response to mid-Aptian sea-level fall. *Cretaceous Research* 27, 814–827.
- 1318
- 1319 Yose, L.A., Strohmenger, C.J., Al-Hosani, I., Bloch, G., Al-Mehairi, Y., 2010.  
1320 Sequence-stratigraphic evolution of an Aptian carbonate platform (Shu'aiba  
1321 Formation), eastern Arabian Plate, onshore Abu Dhabi, United Arab Emirates.  
1322 In: *Barremian – Aptian Stratigraphy and Hydrocarbon Habitat of the Eastern  
1323 Arabian Plate* (Eds. F.S.P. van Buchem, M.I. Al-Husseini, F. Maurer and H.J.  
1324 Droste). *GeoArabia Special Publication* 4, Gulf PetroLink, Bahrain, 2, 309–340.
- 1325
- 1326 Zorina, S.O., 2016. Sea-level and climatic controls on Aptian depositional  
1327 environments of the Eastern Russian Platform. *Palaeogeography,  
1328 Palaeoclimatology, Palaeoecology* 441, 599–609.
- 1329
- 1330 Figure captions:
- 1331 **FIGURE 1** A) Geographical location of the Maestrat, South Iberian and Garraf  
1332 basins in the eastern Iberian Chain (E Iberian Peninsula). B) Simplified  
1333 palaeogeographic and structural map of the Maestrat Basin during the Late  
1334 Jurassic–Early Cretaceous rifting cycle and situation of the Godall Range in the  
1335 eastern Morella Sub-basin. Mo: Morella Sub-basin, Pe: El Perelló Sub-basin,  
1336 Sa: La Salzedella Sub-basin, Ga: Galve Sub-basin, Ol: Oliete Sub-basin, Al:  
1337 Aliaga Sub-basin, Pg: Penyagolosa Sub-basin. Modified after Salas et al.  
1338 (2001).
- 1339
- 1340 **FIGURE 2** Examples of representative constructions in Barcelona where the  
1341 Stone from Ulldecona has been used. The Casa Milà (“La Pedrera”) (A) exhibits  
1342 honed finished pavements made up of Stone from Ulldecona in its inner

1343 courtyards (B). In the Sagrada Família Temple (C), polished Stone from  
1344 Ulldecona was employed to pave the floor of the sacristy (D). The shopping and  
1345 entertainment centre Illa Diagonal (E) is paved with polished and honed (F)  
1346 finished Stone from Ulldecona.

1347

1348 **FIGURE 3** Examples of use of the Stone from Ulldecona in well-known  
1349 buildings in Madrid and Alcalá de Henares. In Madrid, the exterior (A) and  
1350 interior (B) walls of the Spanish Olympic Committee headquarters are clad  
1351 with sandy and honed finished Stone from Ulldecona, respectively. The  
1352 Magisterial Cathedral of Alcalá de Henares (C) is paved with polished and  
1353 honed finished Stone from Ulldecona (D).

1354

1355 **FIGURE 4** Chrono-stratigraphic chart for the Late Barremian-Early Albian of  
1356 the Maestrat Basin including the major transgressive-regressive sequences  
1357 identified in the basin, Sr-derived numerical ages for the different  
1358 lithostratigraphic units, stratigraphic position of the Oceanic Anoxic Event 1a  
1359 (OAE1a) and relevant ammonoid, orbitolinid and rudist occurrences. Different  
1360 species and related stratigraphic ranges are distinguished by using distinct  
1361 colours. Numerical ages, geo-magnetic polarity intervals and ammonoid zones  
1362 are taken from Gradstein et al. (2004). The ammonite zones identified by  
1363 Moreno-Bedmar et al. (2009, 2010, 2012a) and Garcia et al. (2014) are dashed  
1364 in grey. The global transgressive-regressive sequence-stratigraphic framework  
1365 of European basins is taken from Hardenbol et al. (1998). Modified after Bover-  
1366 Arnal et al. (2016).

1367

1368 **FIGURE 5** Geological scheme of the southern part of the Godall Range  
1369 (Grossa Range) with the six cartographic units characterized (key is inset). The  
1370 geological cross-sections (A-A', B-B' and C-C') and the stratigraphic section  
1371 logged are displayed in figure 6 and 7, respectively. The underlying topographic  
1372 map was cropped from the 1:25,000 scale topographic base of Catalonia by the  
1373 *Institut Cartogràfic i Geològic de Catalunya* (sheet 62-41; available at  
1374 <http://www.icgc.cat>).

1375

1376 **FIGURE 6** Simplified geological cross-sections (A-A', B-B' and C-C') showing  
1377 the general structural framework and stratigraphic relationships of the southern  
1378 part of the Godall Range (Grossa Range). The location of cross-sections is  
1379 indicated in Figure 5.

1380

1381 **FIGURE 7** Representative stratigraphic log of the Grossa Range that includes  
1382 ages, lithostratigraphic units, lithologies, textures, dominant skeletal  
1383 components, sedimentological characteristics, a sequence-stratigraphy analysis  
1384 and the stratigraphic position of the interval quarried as an ornamental and  
1385 building stone. This log commences on the TV-3313 road that goes from  
1386 Ulldecona to Godall, with the marl deposits of Forcall Formation (lower Aptian),  
1387 which is the oldest lithostratigraphic unit recognized in the area, and finishes in  
1388 the Mas del Dengo, on a hill adjacent to the road where the basal part of the  
1389 Benassal Formation crops out (uppermost lower Aptian-upper Aptian). The  
1390 location of the stratigraphic column measured in the Grossa Range is indicated  
1391 in Figure 5. The legend of the log is found in Figure 8.

1392

1393 **FIGURE 8** Key to Figure 7.

1394

1395 **FIGURE 9** Representative lithofacies of the lower Aptian of the Grossa  
1396 Range. A) Marls of the Forcall Formation cropping out in the axial part of an  
1397 antiform structure cut by the TV-3313 road. B) Close-up view of *Palorbitolina*  
1398 *lenticularis* specimens found at the base of the Villarroya de los Pinares  
1399 Formation on the TV-3313 road. Scale bar = 2 cm. C) Wackestone with  
1400 fragments of the dasycladale *Salpingoporella muehlbergi* and gastropods of the  
1401 Villarroya de los Pinares Formation quarried as an ornamental and building  
1402 stone in the Grossa Range. Scale bar = 0.5 mm. D) Packstone with miliolids,  
1403 *Orbitolinopsis simplex* and fragments of *Salpingoporella muehlbergi* of the  
1404 Villarroya de los Pinares Formation extracted as an ornamental/building stone  
1405 in the Grossa Range. Scale bar = 0.5 mm. E) Peloidal grainstone with miliolids  
1406 and other foraminifera of the Villarroya de los Pinares Formation quarried as an  
1407 ornamental and building stone in the Grossa Range. Scale bar = 0.5 mm. F)  
1408 Detail of a bioturbated layer extracted as an ornamental stone.

1409

1410 **FIGURE 10** Sedimentary features of the lower part of the Villarroya de los  
1411 Pinares Formation in the Grossa Range. A) Stratigraphic level of the lower part  
1412 of the Villarroya de los Pinares Formation quarried as an ornamental/building  
1413 stone in the southern part of the Godall Range characterized by the presence of  
1414 *Chondrodonta* and rudist bivalves. B) Close-up view of a scleractinian coral  
1415 colony. C) Panoramic view of the lower part of the Villarroya de los Pinares  
1416 Formation quarried as an ornamental/building stone nearby the town of  
1417 Ulldecona. D) Outcrop view within a quarry of a recent karst partially filled with a  
1418 speleothem. Note also how around the fractures and karst affecting the  
1419 dolomitic limestone to calcitic dolostone bed of the upper part of the image,

1420 there is a marked change from dark to a lighter gray colour due to calcitization.  
1421 Scale bar = 1 m.

1422

1423 **FIGURE 11** Characteristic microfossils of the Villarroya de los Pinares  
1424 Formation from the Grossa Range. A) The orbitolinid *Palorbitolina lenticularis*.  
1425 Scale bar = 0.5 mm. B) The orbitolinid *Orbitolinopsis simplex*. Scale bar = 0.5  
1426 mm. C) The orbitolinid *Paracoskinolina maynci*. Scale bar = 0.25 mm. D) The  
1427 benthic foraminifer *Choffatella decipiens*. Scale bar = 0.5 mm. E) The  
1428 microproblematicum *Lithocodium aggregatum*. Scale bar = 0.5 mm. F) The  
1429 dasycladale *Salpingoporella muehlbergi*. Scale bar = 0.25 mm.

1430

1431 **FIGURE 12** Rudist bivalves characteristic of the upper lower Aptian of the  
1432 Grossa Range. A) *Toucasia carinata* from the Villarroya de los Pinares  
1433 Formation. Camera cap = 5.8 cm. B) *Mathesia darderi* from the Villarroya de  
1434 los Pinares Formation. C) *Polyconites*-bearing limestone from the upper part of  
1435 the Villarroya de los Pinares Formation cropping out in a TV-3313 road cut. D)  
1436 Specimens of *Polyconites* sp., most likely *Polyconites hadriani*, from the upper  
1437 part of the Villarroya de los Pinares Formation. Scale bar = 2 cm.

1438

1439 **FIGURE 13** Facies and sedimentology of the top of the Villarroya de los  
1440 Pinares Formation (upper lower Aptian) and the Benassal Formation  
1441 (uppermost lower Aptian-lower upper Aptian) of the Grossa Range. A) Outcrop  
1442 of the transgressive marls of the base of the Benassal Formation in the Mas del  
1443 Dengo. Hammer length = 32 cm. B) Hardground located at the top of the  
1444 Villarroya de los Pinares Formation that marks the drowning of the rudist-  
1445 dominated lower Aptian carbonate platform in Mas del Dengo. Hammer length =  
1446 32 cm. C) Detail of the hardground shown in Fig. 13B. Note the presence of  
1447 borings of lithophagid bivalves and of iron stains. D) Closely-packed cluster of  
1448 *Polyconites* from the upper Aptian Benassal Formation at Mas del Dengo site.  
1449 Camera cap = 5.8 cm.

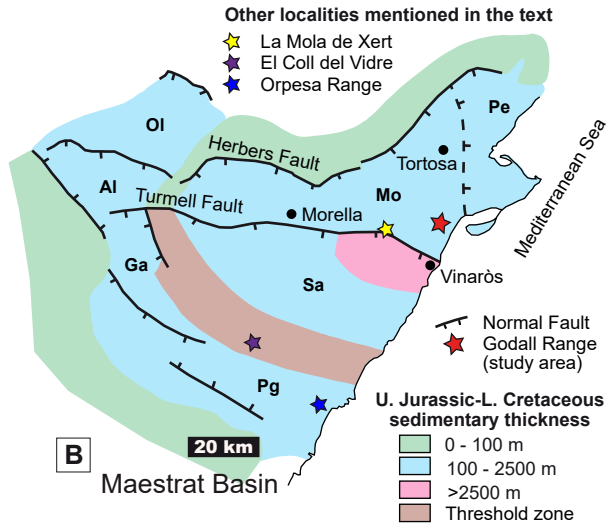
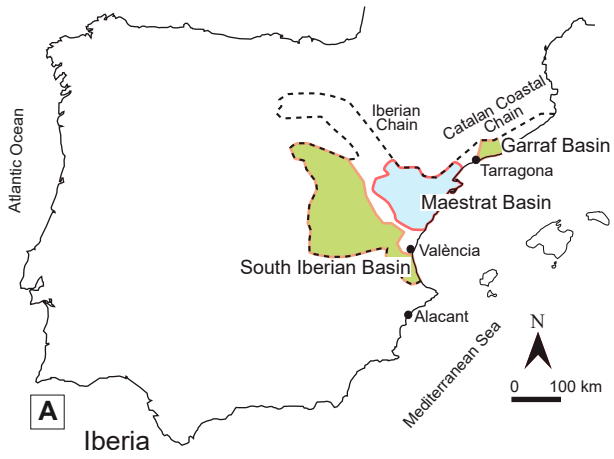
1450

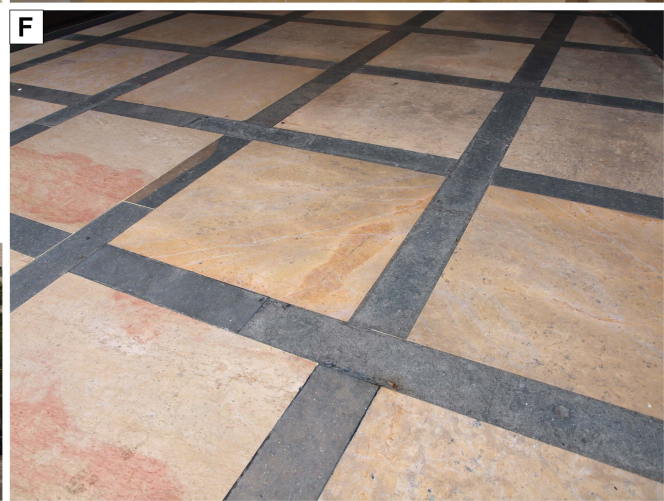
1451 **FIGURE 14** Dolomitization of the lower Aptian platform carbonates of the  
1452 Villarroya de los Pinares Formation in the Grossa Range. A) Laterally  
1453 continuous and thick (ca. 40 m thick) stratabound level of dolostones capping  
1454 the succession commercialized as an ornamental/building stone in the quarries  
1455 of Ulldecona. B) Detail of vacuolar porosity observed in the Sant Joan quarry.  
1456 Camera cap = 5.8 cm. C) Detail of cave porosity photographed in the Sant  
1457 Joan quarry. Scale bar = 1 m. D) Decimetric stratabound levels of dolomitic

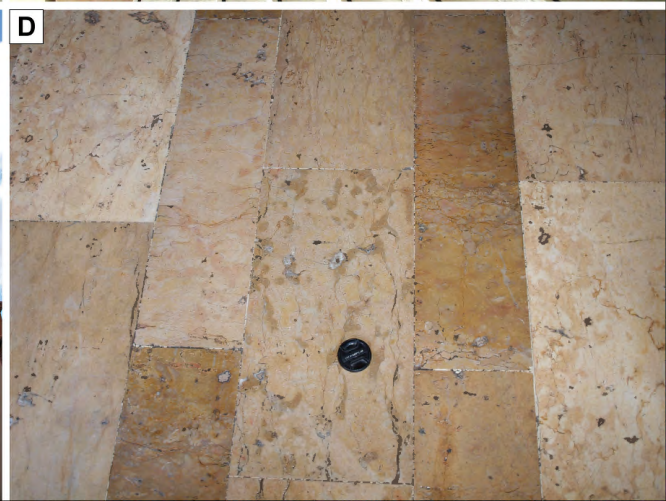
1458 limestone to calcitic dolostone (red arrows) that appear in the lower part of the  
1459 Villarroya de los Pinares Formation in the Sant Joan quarry.

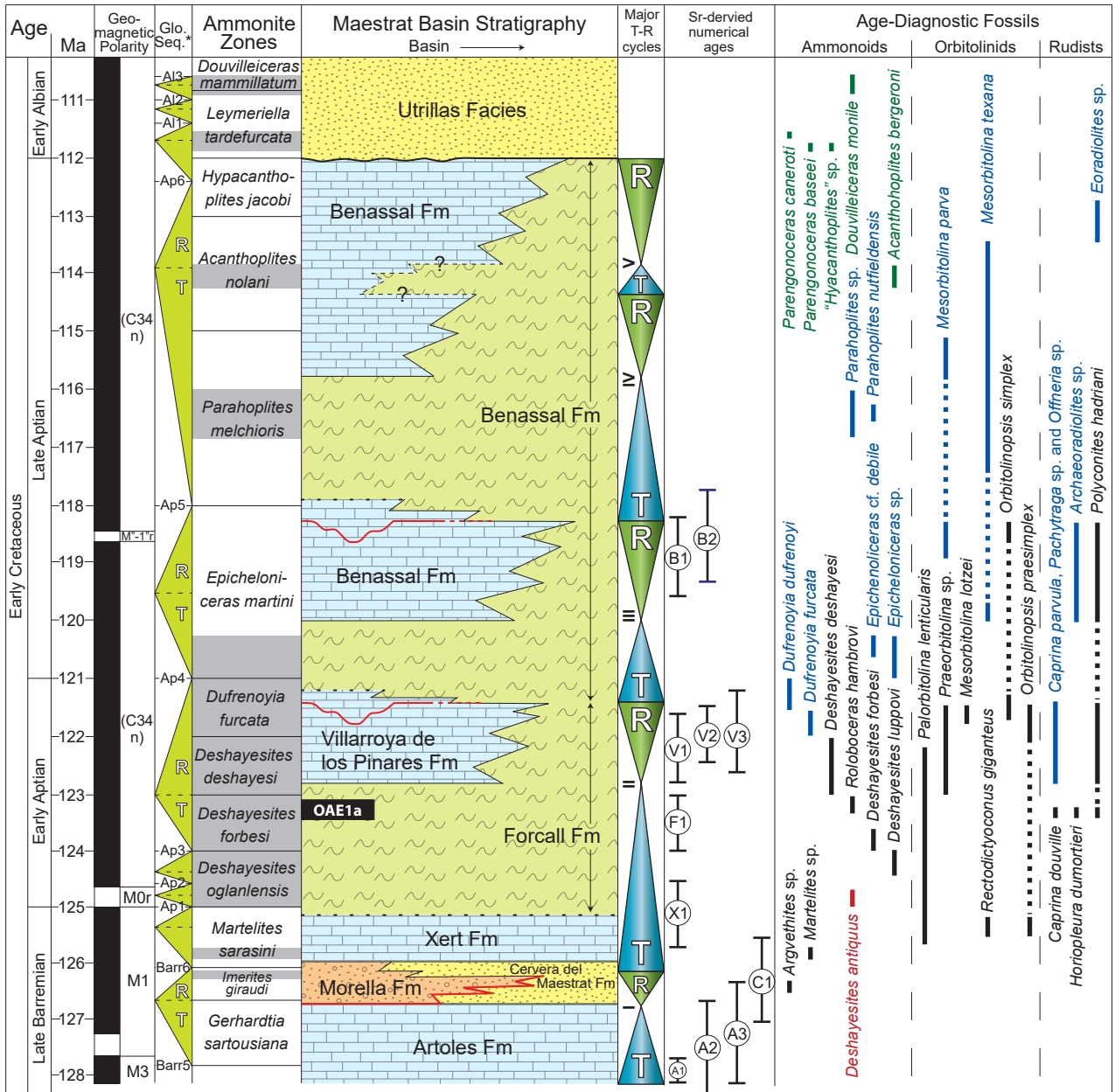
1460

1461 **FIGURE 15** Dolomitization of the lower Aptian platform carbonates of the  
1462 Villarroya de los Pinares Formation in the Grossa Range. A) Initial  
1463 dolomitization stage of a packstone-grainstone texture with peloids and  
1464 orbitolinids. B) Intermediate dolomitization stage of a wackestone-packstone  
1465 texture with miliolids and peloids. C) Idiopic mosaic texture in an advanced  
1466 stage of dolomitization. D) Hypidiopic mosaic texture in an advanced stage of  
1467 dolomitization. Scale bars = 0.5 mm.



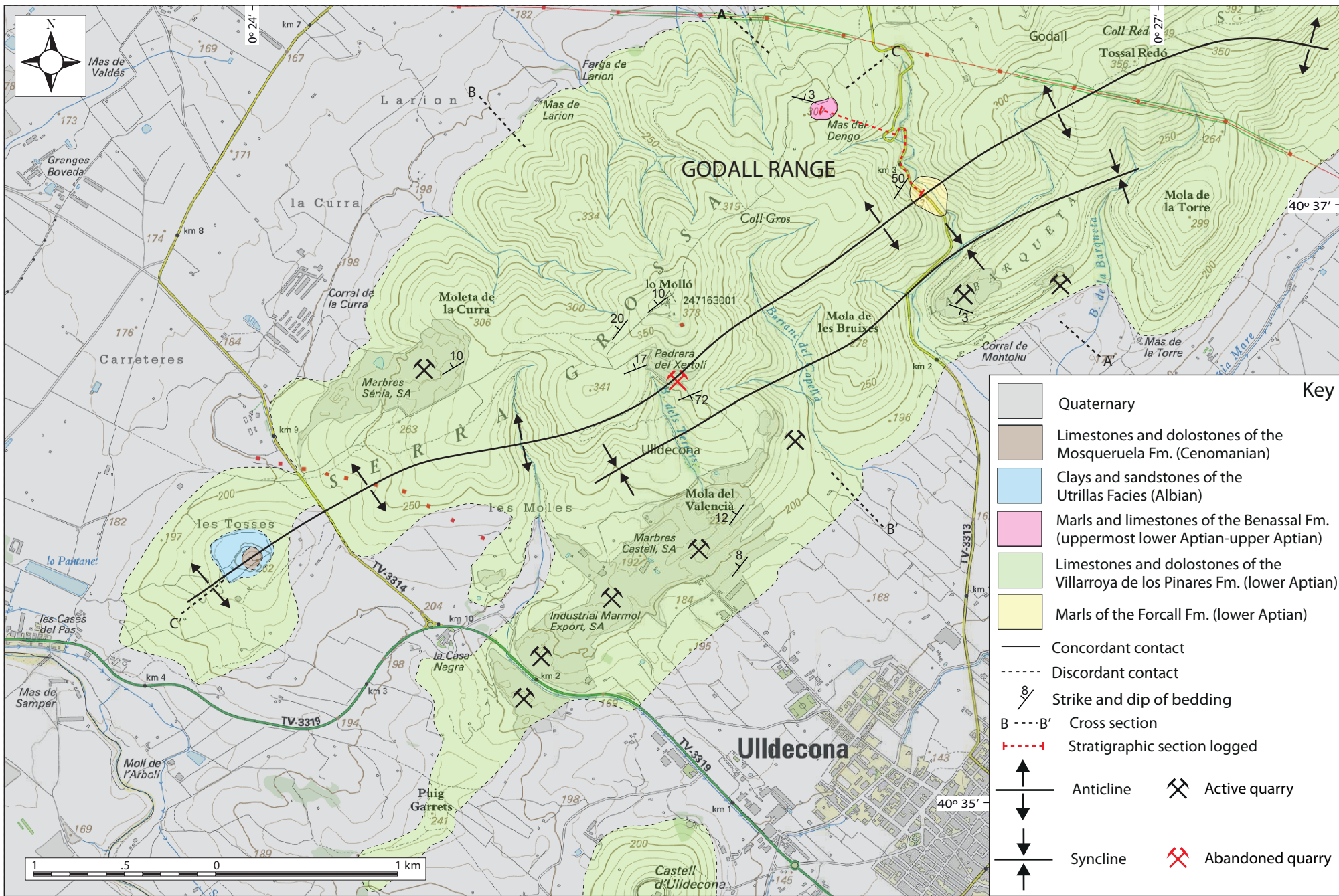






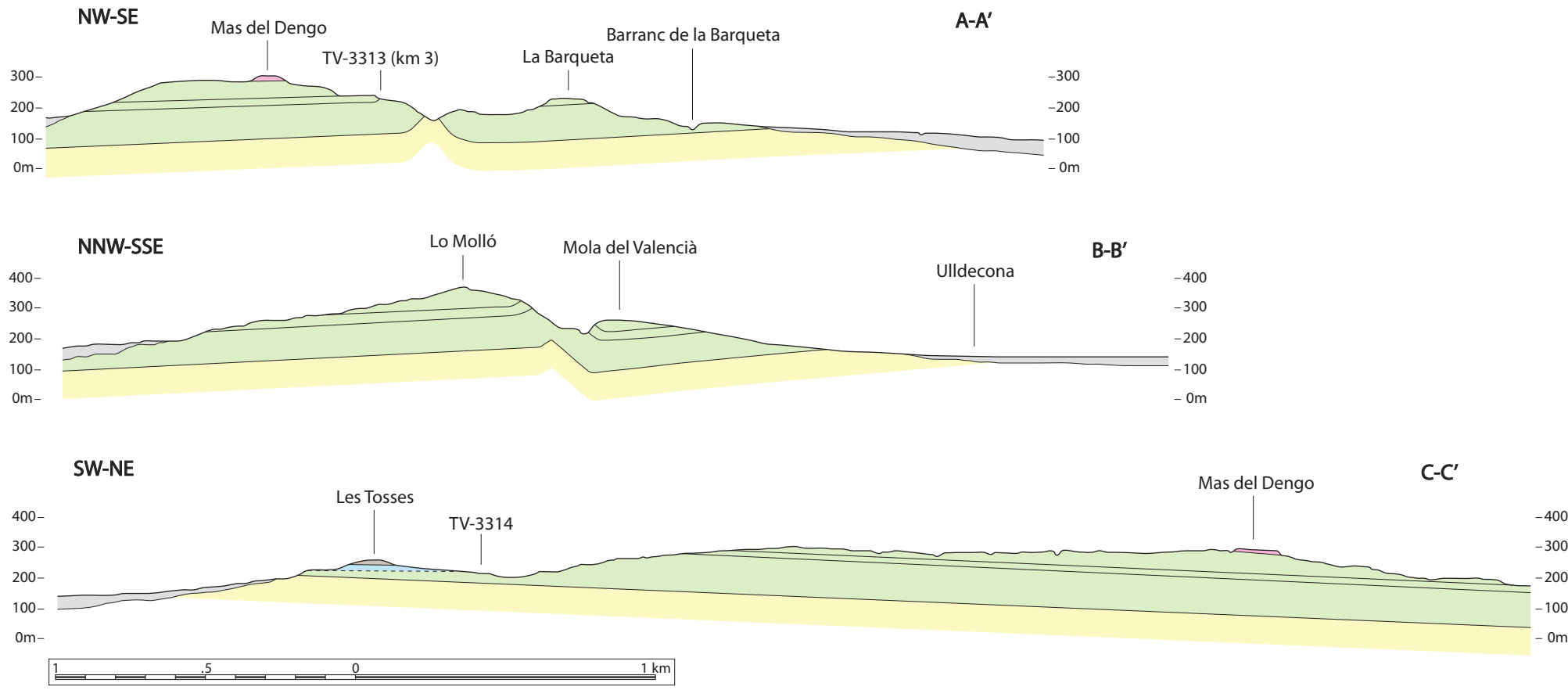
	Basal marine marls and limestones		Continental clastics
	Platform and transitional limestones, sandy limestones and marls		Coastal and shallow-subtidal clastics
	Correlative conformity		Erosional unconformity
	Lithostratigraphic boundary lacking absolute dating		Surface of subaerial exposure
	Sr-derived absolute numerical age range		Drowning surface
			Deeply incised subaerial unconformity
A1-3	Samples collected in the Artoles Formation, Salzedella sub-basin	T	Transgressive
C1	Sample collected in the Cervera del Maestrat Formation, Salzedella sub-basin	R	Regressive
X1	Sample collected in the Xert Formation, Salzedella sub-basin		
F1	Sample collected in the Forcall Formation, Galve sub-basin		
V1-3	Samples collected in the Villarroya de los Pinares Formation, Galve sub-basin		
B1-2	Samples collected in the Benassal Formation, Galve and Morella sub-basins		

\*Global Sequences (Hardenbol et al. 1998, Gradstein et al. 2004)



**Key**

- Quaternary
- Limestones and dolostones of the Mosqueruela Fm. (Cenomanian)
- Clays and sandstones of the Utrillas Facies (Albian)
- Marls and limestones of the Benassal Fm. (uppermost lower Aptian-upper Aptian)
- Limestones and dolostones of the Villarroya de los Pinares Fm. (lower Aptian)
- Marls of the Forcall Fm. (lower Aptian)
- Concordant contact
- Discordant contact
- 8  
/ Strike and dip of bedding
- B --- B' Cross section
- Stratigraphic section logged
- ↑  
↓ Anticline
- ↓  
↑ Syncline
- ⚒ Active quarry
- ⚒ Abandoned quarry



**Key**



- Concordant contact
- - - - - Discordant contact

- Limestones and dolostones of the Villarroya de los Pinares Fm. (lower Aptian)
- Marls of the Forcall Fm. (lower Aptian)



### Stratigraphic log's key:

-  Marl
-  Marly-limestone
-  Limestone
-  Dolomitic limestone
-  Calcitic dolomite and dolostone
- MRS    Maximum regressive surface
-  Perforated hardground
-  Nodular stratification

-  Facies-characteristic component
-  Common component or presence of bioturbation structures
-  Rare component
-  Mouldic porosity
-  Transgression
-  Regression
- MFS    Maximum flooding surface
-  Iron crust
-  *Chondrodonta* and/or elevator rudists in life position

